THERMAL MEASUREMENTS and INVERSE TECHNIQUES

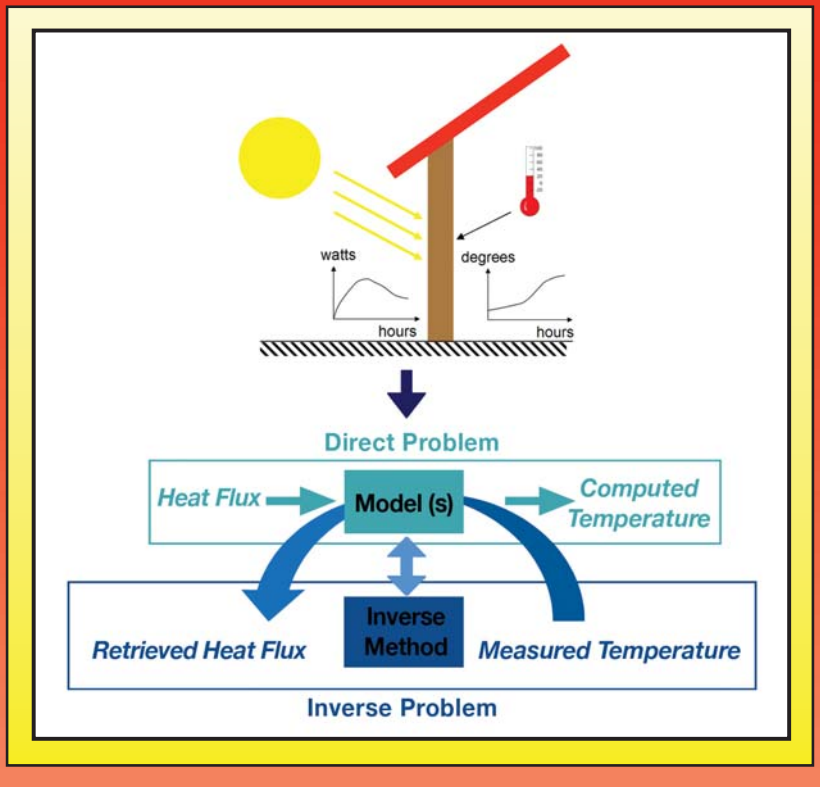

Edited by

Helcio R.B. Orlande • Olivier Fudym

Denis Maillet • Renato M. Cotta

CRC Press
Taylor & Francis Group

THERMAL MEASUREMENTS and INVERSE TECHNIQUES

HEAT TRANSFER

A Series of Reference Books and Textbooks

Editor

Afshin J. Ghajar

Regents Professor
School of Mechanical and Aerospace Engineering
Oklahoma State University

Engineering Heat Transfer: Third Edition, *William S. Janna*

Conjugate Problems in Convective Heat Transfer, *Abram S. Dorfman*

Thermal Measurements and Inverse Techniques, *Helcio R.B. Orlande; Olivier Fudym; Denis Maillet; Renato M. Cotta*

Upcoming titles include:

Introduction to Thermal and Fluid Engineering, *Allan D. Kraus, James R. Welty, and Abdul Aziz*

THERMAL MEASUREMENTS and INVERSE TECHNIQUES

Edited by
Helcio R.B. Orlande
Olivier Fudym
Denis Maillet
Renato M. Cotta

CRC Press
Taylor & Francis Group
Boca Raton London New York

CRC Press is an imprint of the
Taylor & Francis Group, an **informa** business

CRC Press
Taylor & Francis Group
6000 Broken Sound Parkway NW, Suite 300
Boca Raton, FL 33487-2742

Version Date: 20140602

International Standard Book Number-13: 978-1-4398-4556-1 (eBook - PDF)

Contents

Preface

The design and operation of modern technological systems and the proper comprehension of their interaction with nature (e.g., in pollution control and global warming issues) require the permanent processing of a large amount of measured data. Nowadays, progress in the mathematical modeling of complex industrial or environmental systems, associated with the continuous increase in memory and calculation power of computers, has made numerical simulations of almost any physical phenomena possible. These facts bring about the need for an appropriate tool that rigorously bridges the gap between the information stemming from measurements and that corresponding to theoretical predictions, aiming at the better understanding of physical problems, including real-time applications. Inverse analysis is such a tool.

Heat transfer permanently takes part in our daily life. Examples can be found in natural phenomena, such as the solar heating of Earth, meteorology or thermoregulation of biological activity, as well as in a wide range of man-made applications, such as the conversion of energy in heat engines, thermal control of chemical reactors, air conditioning, cooling of electronic equipment, development of micro- and nano-technologies with the associated thermal challenges, etc. Recent advances in both thermal instrumentation and heat transfer modeling permit the combination of efficient experimental procedures and of indirect measurements within the research paradigm of inverse problems. In this paradigm, the groups of theoretical, computational, and experimental researchers synergistically interact during the course of the work in order to better understand the physical phenomena under study. Although initially associated with the estimation of boundary heat fluxes by using temperature measurements taken inside a heated body, inverse analyses are nowadays encountered in single- and multi-mode heat transfer problems dealing with multiscale phenomena. Applications range from the estimation of constant heat transfer parameters to the mapping of spatially and timely varying functions, such as heat sources, fluxes, and thermophysical properties.

In heat transfer, the classical inverse problem of estimating a boundary heat flux with temperature measurements taken inside a heat-conducting medium has many practical applications. For example, the heat load of the surface of a space vehicle reentering the atmosphere can be estimated through inverse analysis by using temperature measurements taken within the thermal protection shield. If a technique that sequentially estimates such boundary heat flux is used, inverse analysis may allow for online trajectory corrections in order to reduce the heat load. Therefore, overheating of the structure of the spacecraft can be avoided, reducing the risk of fatal accidents. Moreover, modern engineering strongly relies on newly developed materials, such as composites, and inverse analysis can be used for the characterization of the unknown properties of such nonhomogeneous materials. The use of nonintrusive measurement techniques with high spatial resolutions and high measurement frequencies, such as temperature measurements taken

with infrared cameras, allows the characterization of nonhomogeneous materials even at small scales, including crack or defect detection. The latest research in heat transfer follows a trend toward small scales, at micro- and nano-levels. This requires that physical phenomena be taken into consideration, which may be negligible and, hence, not accounted for at macroscales. By the same token, modern techniques now permit nonintrusive measurements to be taken at small space and time scales, thus allowing the observation of such complex physical phenomena.

All subjects required for the understanding and solution of the physical situations described above are available in this book, including the modeling of heat transfer problems, even at micro- and nano-scales, modern measurement techniques, and the solution of inverse problems by using classical and novel approaches. This book is aimed at engineers, senior undergraduate students, graduate students, researchers both in academia and industry, in the broad field of heat transfer. It is assumed, however, that the reader has basic knowledge on heat transfer, such as that contained in an undergraduate heat transfer course.

This book is intended to be a one-source reference for those involved with different aspects of heat transfer, including the modeling of physical problems, the measurement of primary heat transfer variables, and the estimation of quantities appearing in the formulation (indirect measurements) through the solution of inverse problems. Keeping this main objective in mind, the book was divided into three parts, namely: Part I—Modeling and Measurements in Heat Transfer, Part II—Inverse Heat Transfer Problems, and Part III—Applications. Parts I and II provide a concise theoretical background along with examples on modeling, measurements, and solutions of inverse problems in heat transfer. Part III deals with applications of the knowledge built up in Parts I and II to several practical test cases. Each chapter contains its own lists of variables and references. Hence, depending on the reader's background and interest, they can be read independently.

This book results from the Advanced Schools METTI (Thermal Measurements and Inverse Techniques) held in 1995, 1999, 2005, and 2009. Started under the auspices of SFT—French Heat Transfer Society, the last METTI School was co-organized with ABCM—Brazilian Society of Mechanical Engineering and Sciences, and held in Angra dos Reis (state of Rio de Janeiro) as one of the activities of the Year of France in Brazil. However, the book was intended to be self-consistent and didactic, not being at all the single collection of lectures previously given during the METTI schools.

We would like to thank all the contributors for their diligent work that made this book possible. We are indebted to Professor Afshin J. Ghajar, the Heat Transfer series editor for CRC Press/Taylor & Francis, for his encouragement and support to pursue this book project. We also appreciate the valuable recommendation by Professor Sadik Kakac, who carefully reviewed our book proposal. The cooperation of the staff at CRC Press/Taylor & Francis is greatly appreciated, especially that from Jonathan W. Plant, the senior editor for mechanical, aerospace, nuclear, and energy engineering, and from our project coordinator, Amber Donley. Finally, we would like to express our deepest gratitude for the financial support provided for the publication of this book by CAPES, an agency of the Brazilian government for the fostering of science and graduate studies.

For MATLAB® and Simulink® product information, please contact:

The MathWorks, Inc.
3 Apple Hill Drive
Natick, MA, 01760-2098 USA
Tel: 508-647-7000
Fax: 508-647-7001
E-mail: info@mathworks.com
Web: www.mathworks.com

Contributors

Stéphane Andre
Energy and Theoretic and Applied Energy Laboratory (LEMTA)
University of Nancy and CNRS
Vandœuvre-lès-Nancy, France

Liliane Basso Barichello
Institute of Mathematics
Federal University of Rio Grande do Sul
Porto Alegre, Brazil

Elena Palomo del Barrio
TREFLE Laboratory
Ecole Nationale Supérieure des Arts et Métiers
University of Bordeaux
Talence, France

Jean-Christophe Batsale
TREFLE Laboratory
Ecole Nationale Supérieure des Arts et Métiers
University of Bordeaux
Talence, France

Jean-Luc Battaglia
TREFLE Laboratory
Ecole Nationale Supérieure des Arts et Métiers
University of Bordeaux
Talence, France

Valério L. Borges
School of Mechanical Engineering
Federal University of Uberlândia
Uberlândia, Brazil

Marcelo J. Colaço
Department of Mechanical Engineering
Federal University of Rio de Janeiro
Rio de Janeiro, Brazil

Renato M. Cotta
Department of Mechanical Engineering
Federal University of Rio de Janeiro
Rio de Janeiro, Brazil

Manuel Ernani Cruz
Department of Mechanical Engineering
Federal University of Rio de Janeiro
Rio de Janeiro, Brazil

Morgan Dal
Materials Engineering Laboratory of Brittany (LIMATB)
University of Southern Brittany
Lorient, France

Jean-Luc Dauvergne
TREFLE Laboratory
Ecole Nationale Supérieure des Arts et Métiers
Talence, France

George S. Dulikravich
Department of Mechanical and Materials Engineering
Florida International University
Miami, Florida

Ana P. Fernandes
School of Mechanical Engineering
Federal University of Uberlândia
Uberlândia, Brazil

Olivier Fudym
Research in Albi on Particulate Solids, Energy and the Environment
University of Toulouse
Albi, France

Eric Gavignet
Department of Energy & Engineering of Multiphysic Systems
FEMTO-ST
University of Franche-Comté
Belfort, France

Manuel Girault
Department of Fluid, Thermal and Combustion Sciences
PPRIME Institute
Chasseneuil-du-Poitou, France

Gilmar Guimarães
School of Mechanical Engineering
Federal University of Uberlândia
Uberlândia, Brazil

Saulo Güths
Department of Mechanical Engineering
Federal University of Santa Catarina
Florianópolis, Brazil

Yvon Jarny
Department of Thermal and Energy Sciences
Polytechnic School of the University of Nantes
Nantes, France

Jean-Claude Krapez
Department of Theoretical and Applied Optics
ONERA—The French Aerospace Lab
Salon de Provence, France

François Lanzetta
Department of Energy & Engineering of Multiphysic Systems
FEMTO-ST
University of Franche-Comté
Belfort, France

Denis Maillet
Energy and Theoretic and Applied Energy Laboratory
National Center for Scientific Research
University of Nancy
Vandœuvre-lès-Nancy, France

Philippe Le Masson
Materials Engineering Laboratory of Brittany (LIMATB)
University of Southern Brittany
Lorient, France

Carlos Frederico Matt
Department of Equipment and Installations
Electric Power Research Center
Rio de Janeiro, Brazil

Thomas Metzger
Thermal Process Engineering
Otto-von-Guericke University
Magdeburg, Germany

Luís Mauro Moura
Thermal System Laboratory
Pontifical University Catholic of Paraná
Curitiba, Brazil

Carolina P. Naveira-Cotta
Department of Mechanical Engineering
Federal University of Rio de Janeiro
Rio de Janeiro, Brazil

Christophe Le Niliot
University Institute of Industrial Thermal Systems (IUSTI)
Technopole de Château Gombert
Marseille, France

Helcio R. Barreto Orlande
Department of Mechanical Engineering
Federal University of Rio de Janeiro
Rio de Janeiro, Brazil

Marina Silva Paez
Department of Statistical Methods
Federal University of Rio de Janeiro
Rio de Janeiro, Brazil

Daniel Petit
Department of Fluid, Thermal and Combustion Sciences
PPRIME Institute
Chasseneuil-du-Poitou, France

Benjamin Remy
Energy and Theoretic and Applied Energy Laboratory (LEMTA)
University of Nancy and CNRS
Vandœuvre-lès-Nancy, France

Fabrice Rigollet
University Institute of Industrial Thermal Systems (IUSTI)
Technopole de Château Gombert
Marseille, France

Paulo Seleghim, Jr.
Mechanical Engineering Department
University of São Paulo
São Carlos, Brazil

Priscila F.B. Sousa
School of Mechanical Engineering
Federal University of Uberlândia
Uberlândia, Brazil

Haroldo F. de Campos Velho
Laboratory of Computing and Applied Mathematics
National Institute for Space Research
São José dos Campos, Brazil

Etienne Videcoq
Department of Fluid, Thermal and Combustion Sciences
PPRIME Institute
Chasseneuil-du-Poitou, France

Part I

Modeling and Measurements in Heat Transfer

1

Modeling in Heat Transfer

Jean-Luc Battaglia and Denis Maillet

CONTENTS

1.1 Introduction

Modeling constitutes a very general activity in engineering. A system can be considered as modeled if its behavior or its response to a given excitation can be predicted. So prediction is one of the natural characteristics of modeling.

In the second section of this chapter, the basics on heat transfer physics are presented. The existence of temperature and more specifically of temperature gradient must be discussed carefully when time and length scales become very small. This is the case for new applications in the field of inverse heat conduction problems. This point is known for a long time at very low temperature. It becomes also particularly true at the nanoscale when temperature is greater than the Debye temperature (above this temperature, the quantum effects are generally neglected). Classical Fourier's law, at the basis of standard heat transfer models, is no longer valid, and either a new model or a definition of the reliable time range for the pertinent use of Fourier's law is thus required. In the third section of this chapter, the concept of homogenization for heterogeneous materials through macroscopic homogenized models is presented. This topic is also studied in Chapter 2. An illustration of such a problem is represented in Figure 1.1.

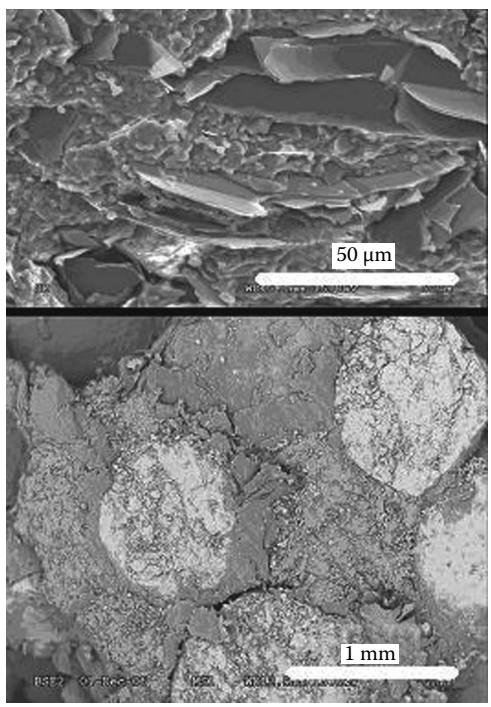

FIGURE 1.1
Phase change material for energy storage (double porosity carbon graphite/salt porous media with phase change material [PCM]). Scanning electron microscopy (SEM) imaging illustrates different heterogeneity levels according to the observation scale and shows that a specific model is required for each.

Another important feature of a model, which is only a theoretical representation of the physical reality in the case of a material system, is its structure (we do not deal here with information systems). In heat transfer, the choice is quite large, and the model structure should be selected according to the objective of the model. The model-builder can have in mind an optimal design problem, a parameter estimation problem using measurements, a control problem to define the best excitation shape for a given desired output, or a model reduction problem, just to quote a few applications.

The choice of the structure of a model in heat transfer depends on many things:

- State variable and observed quantities
  In a heat diffusion problem, temperature is the quantity that constitutes the state variable, in the thermodynamics sense. In order to calculate temperature and heat flux at any time t and at any point P, one has to know the initial temperature field (at time $t = 0$) at the local scale, as well as the history of the different thermal disturbances between times 0 and t. So, one has to define what is a *local* point P and a local scale. For instance, if heat transfer is intended to be studied at the very small scale in a metal (smaller than the grain size), Fourier's law, relating heat flux to temperature gradient, may no longer be valid. In such a case, two temperatures (respectively for the electron gas and the lattice) are required to describe heat transfer at this scale (see Section 1.2.3). Such a *detailed* state model will be necessary if *observations* or predictions are looked for at the nanoscale or at the picosecond timescale. The upper thresholds of both scales depend on the considered material. A similar effect appears in a heterogeneous medium composed of two homogeneous materials (grains made of one material embedded in a matrix made of the other material, for example): instead of using temperature at the local scale (grain or matrix), some averaging, that is a space filtering, will be used at the macroscopic scale (see Sections 1.3 and 1.4 and Chapter 2).
- State definition
  The continuous state equations have then to be defined for the modeling problem at stake: it can be a partial differential equation, the heat equation (state = temperature), or an integro-differential equation, the radiative transfer equation (state = radiative intensity), or both coupled equations. Their solution, that is constituted by both temperature and intensity fields in the third case, should be calculated everywhere and any time past the initial time (see Section 1.5.2).
- Quantities of the direct problem
  We focus on the diffusion heat equation in a medium composed of one or several homogeneous materials, with its associated initial, boundary, and interface equations. Its solution, the state variable, here the continuous temperature field $T(\mathrm{P}, t)$, has first to be found, and the desired observed quantities, that is, the (theoretical) output of the model at a given point P, $y_{mo}(t) = T(\mathrm{P}, t)$, have to be calculated next (see Section 1.5.1). Here the quantities that are required for solving the *direct problem* are the structural parameters of the system (conductivities, volumetric heat capacities, heat exchange coefficients, emissivities of walls, ...), the thermal excitation, and the initial temperature field $T(\mathrm{P}, t = 0)$. Let us note here that it is possible to make a *physical reduction* of a model based on the three-dimensional (3D) transient heat equation to get simpler models of lower dimensionality. The thermal fin (1D) or the bulk temperature (0D) types (see Section 1.6.2) constitute such reduced models. This type of reduction may also reduce the number of parameters defining the excitations.

- Numerical/analytical model
  There are many ways for solving the heat equation and finding a *state model* for the observations: *analytical solutions* provide the temperature field explicitly as a function of the structural parameters of the system, the excitation, and the initial state. They can be constructed if the heat equation in each material and the associated conditions are all linear and the corresponding geometry simple. The other class of state models relies on the *discrete formulation* of the heat equation: one can quote the nodal, boundary element, finite elements, and finite volume methods, for example. State models rely on an internal representation of the system: the temperature field has to be found first and the observations are calculated next. External representations that short circuit the state variable and link directly the observation to the excitation(s), for example, through a time or space transfer function, in the linear case, constitute another class of models (see Section 1.5.2.1).
- Parameterization for inverse problem solution
  Parameterization of the data of the direct problem constitutes another characteristic of the structure of a model: structural parameters, thermal excitations, and the initial temperature field are, in the very general case, functions of different explanatory variables: space, time, and temperature. The conversion of functions into vectors of finite dimensions does not involve any problem in the *direct problem* (calculation of the observations, the model output, as a function of the input). It is no more the case when the *inverse problem* is considered. This point will be discussed in Section 1.5.2.2. The interested reader can also consult Chapter 14, where reduction of experimental data is studied. One of the objectives of *mathematical reduction* methods is to construct a *reduced model* that will have a reduced number of structural parameters, starting from a *detailed reference model* (see Chapter 13 for details on model reduction), while *physical reduction* also changes the definitions of both output and excitations (see Section 1.6.2).

1.2 Pertinent Definition of a Direct Model for Inversion of Measurements

1.2.1 Heat Conduction at the Macroscopic Level

Heat transfer by diffusion takes place in solids and motionless fluids and was mathematically described for the first time by Joseph Fourier (1828) in his ''Mémoire sur la théorie analytique de la chaleur'' (Treatise on the analytical theory of heat). Fourier's relation is phenomenological, that is, derived experimentally. It relates the heat flux density (a vector) to the temperature gradient inside the material under the form of the following linear relationship:

$$\vec{\varphi} = -k\overrightarrow{\nabla} T \tag{1.1}$$

where operator $\overrightarrow{\nabla} T = (\partial T/\partial x, \partial T/\partial y, \partial T/\partial z)$ denotes the temperature gradient. Consequently, the heat flow rate $\mathrm{d}\phi$ traversing an elementary surface of area $\mathrm{d}S$, centered at this location with an orientation defined by a unit length outward pointing vector $\vec{n}$, is

$$\mathrm{d}\phi = \varphi_n \,\mathrm{d}S \quad \text{with } \varphi_n = \vec{\varphi} \cdot \vec{n} = -k\overrightarrow{\nabla} T \cdot \vec{n} \tag{1.2}$$

where

the direction of $\vec{n}$ is arbitrary (two choices are possible)

φ_n is the normal flux (a scalar, sometimes called normal flux density) expressed in W m^{-2}

In order to recover the heat flux ϕ (W) going through a finite surface (not necessary planar) of area S, Equation 1.2 has to be integrated over its whole area. In the particular case of a one-dimensional heat transfer through a planar surface of area S, normal to the x-direction (a cross section), the heat flux is

$$\phi = -kS\frac{\partial T}{\partial x} \tag{1.3}$$

Finally, k is defined as the thermal conductivity of the material. It can be viewed as an intrinsic thermal property of the material. However, it is expressed from more fundamental quantities such as the mean free path of heat carriers (phonons, electrons, and fluid particles), the velocity group as well as fundamental constants (the reduced Planck constant $\hbar$ and the Boltzmann constant k_B).

In many cases encountered in nature or in man-made objects, thermal conductivity is no longer isotropic but orthotropic, or more generally anisotropic. In the orthotropic case (for composite materials, for example, and in the principal axes of the tensor), Fourier's law becomes

$$\vec{\varphi} = -k_x\frac{\partial T}{\partial x}\vec{x} - k_y\frac{\partial T}{\partial y}\vec{y} - k_z\frac{\partial T}{\partial y}\vec{z} \tag{1.4}$$

The three components of the heat flux are expressed according to the three corresponding values for the thermal conductivity in each direction. In case of an anisotropic medium, the symmetrical thermal conductivity tensor can be introduced:

$$\overline{\overline{k}} = \begin{bmatrix} k_{xx} & k_{xy} & k_{xz} \\ & k_{yy} & k_{yz} \\ \text{sym} & & k_{zz} \end{bmatrix} \tag{1.5}$$

Thermal conductivity of materials can vary significantly with temperature. In a general manner, materials act as superconductors at very low temperature (in the 1–10 K temperature range) whereas the thermal conductivity decreases as the temperature increases. The thermal conductivity varies slightly when temperature is greater than the Debye temperature up to the phase change. In the molten state, the thermal conductivity does not change significantly, but in such a configuration, heat transport by convection becomes as important as conduction.

Thermal diffusivity is defined as the ratio of the thermal conductivity and the specific heat per unit volume:

$$a = \frac{k}{\rho c_p} \tag{1.6}$$

It is thus possible to estimate the diffusion time $t_{diff} = L^2/a$ when heat diffuses in the direction defined by its characteristic length L as reported in Table 1.1.

TABLE 1.1

Characteristic Diffusion Times (Thermal Diffusivity Is $a = 10^{-6}$ m^2 s^{-1})

L	Sphere (Radius 6400 km)	0.3 m	1 cm	100 nm	1 nm
t_{diff}	10^{12} years	10^5 s	100 s	10^{-8} s	10^{-12} s = 1 ps

Fourier's law becomes unappropriate to simulate heat transfer by conduction at very short times of the order of the picosecond that are related to the nanoscale (according to Table 1.1). If one considers the response to a localized heat pulse on the material, Fourier's law shows that the temperature field is modified instantaneously at every point of space since the pulse start. However, at a later time t, temperature cannot have been modified beyond a distance equal to the quantity: $c\,t$, otherwise the effect of the pulse would have propagated faster than the speed of light c. The relationship relating heat flux and temperature gradient must therefore be modified. It has been done by Caetano who introduced a form involving a relaxation time τ:

$$\tau \frac{\partial \vec{\varphi}}{\partial t} + \vec{\varphi} = -k\vec{\nabla}T \tag{1.7}$$

This relaxation time τ depends on the nature of the heat carriers (phonons, electrons, or fluid particles) and more generally on the collision processes between them.

Equivalently, we may compare a characteristic length scale for evolution of the system with the other intrinsic property: the mean free path of the heat carriers. If the latter is much greater than the characteristic length of the medium, the local Fourier law is no longer valid.

1.2.2 An Experimental Observation

Before presenting theoretical developments, it would be interesting to start with an experimental result obtained using the femtoseconds (1 fs = 10^{-15} s) time domain thermoreflectance (TDTR) technique. This experiment consists in applying a very short pulse (some tenths of femtoseconds) at the front face of a material and to measure the transient temperature response on the heated area (see Figure 1.2). The pulse laser is called the pump. A probe laser beam is focused on the heated area, and a photodiode allows measuring the reflected beam intensity from the surface. Since the intensity of the reflected beam is known to vary linearly with temperature (for small pump intensity), the measured signal is proportional to the variation of the time-dependent surface temperature. An ad hoc postprocessing of the output signal allows building a normalized impulse response for the sample.

This experiment is known as the front face method (the thermal disturbance and the temperature measurement are realized at the same location). In a sense, the TDTR can be viewed as an extension of the classical ''flash'' method for very short times. In the experimental configuration described in Figure 1.2, the TDTR technique is used for characterizing a very thin layer (100 nm thick) of a semiconducting alloy: $Ge_2Sb_2Te_5$ (commonly denoted GST) whose thermal effusivity is $b_{GST} = \sqrt{k_{GST}(\rho c_p)_{GST}}$. A thermal

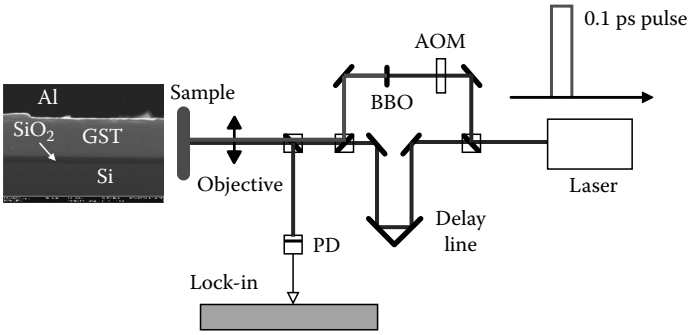

FIGURE 1.2
Radiation of pump is doubled by a β-BaB_2O_4 (BBO) nonlinear optical crystal. The probe pulse is delayed according to the pump pulse up to 7 ns with a temporal precision of a few tens of femtoseconds by means of a variable optical path. The pump beam, whose optical path length remains constant during the experiment, is modulated at a given frequency of 0.3 MHz by an acousto-optic modulator (AOM). In order to increase the signal over noise ratio, a lock-in amplifier synchronized with the modulation frequency is used. Probe and pump beams have a Gaussian profile. The experimental setup is described in Battaglia et al. (2007). An example of sample is represented on the SEM image; the Al layer is used as a thermal transducer to absorb the incident radiation of the pump.

transducer is an aluminum film (denoted Al), of thickness e_{Al} and specific heat per unit volume $(\rho c_p)_{\mathrm{Al}}$, deposited on the GST layer in order to increase the signal–noise ratio during the TDTR experiment. For the duration of the experiment (a tenth of nanoseconds), the GST layer is viewed as a semi-infinite medium. Using the classical heat diffusion model, based on Fourier's law, an analytical expression is obtained for the average (with respect to the spatial distribution of temperature on the heated area) normalized impulse response as follows:

$$\overline{TDTR} = \exp\left(\frac{t}{t_c}\right)\mathrm{erfc}\left(\sqrt{\frac{t}{t_c}}\right) \quad \text{with } t_c = \left(\frac{e_{Al}(\rho c_p)_{\mathrm{Al}}}{b_{GST}}\right)^2 \tag{1.8}$$

Experimental measurements are reported in Figure 1.3, as well as the simulation obtained from the analytical solution (1.8).

It clearly appears that the measured impulse response fits very well with the simulated semi-infinite behavior when time becomes higher than $t_c = 0.3\,\mathrm{ns}$. This result comes from the fact that thermal equilibrium, also called thermalization, between the electrons gas and the lattice in the aluminum film must be taken into account in the model for short times just after the pulse. This effect can be modeled through a specific model: the two-temperature model (see Section 1.2.3.4). This time is defined as the thermalization time of the heat carriers: electrons and phonons. It can be viewed as the relaxation time that has been introduced in Equation 1.6. However, as it will be shown in Section 1.2.3.4, the relaxation time τ is lower than time t_c, estimated from Figure 1.3, since the thermal resistance at the Al–GST interface was not taken into account in this equation.

This observation leads us to take care of the direct model formulation that will be used to solve an inverse problem. It should be adapted to the timescale concerned within the experiment. Indeed, in the example presented above, one can only estimate the thermal effusivity of the layer for time t such as $t > t_c$. This last point has a significance since the

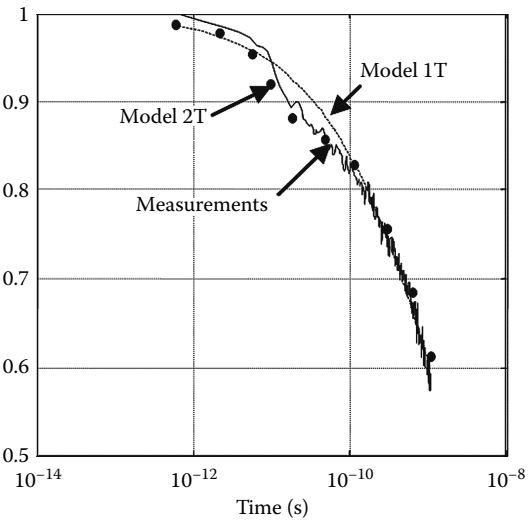

FIGURE 1.3
Impulse response obtained using the TDTR experiment on a GST layer capped with an Al transducer. Plain line is the measurement from 1 ps up to 2 ns. The dotted line is the simulation using the Fourier law (Model 1T), and the plain circles are obtained from the simulation of the two-temperature model (Model 2T, described later in this text).

concepts of thermal conductivity and even of temperature do not make sense anymore at the very small scales. Finally, it is also clear that different thermal parameters, in terms of their physical meaning, will be introduced according to the direct model formulation.

1.2.3 How Can Heat Transfer Be Modeled at the Nanoscale?

1.2.3.1 Discussion

We have highlighted above the intimate link between temperature gradient and mean free path of the carriers in solids: phonons and electrons. In particular, if the characteristic dimension of the material is smaller than the mean free path Λ of these carriers, only a thermal conductance K can be used for relating heat flux to the temperature difference ΔT at the material surface as $\varphi = K\Delta T$. In other words, expressing the thermal conductance as the classical ratio k/e when $e \leq \Lambda$ does not make any sense (see Figure 1.4).

Nevertheless, current challenges for miniaturization force engineers to implement materials in structures whose dimensions lie between several nanometers and a few hundreds of nanometers (see Figure 1.5). Study of the heat transfer in these structures requires using

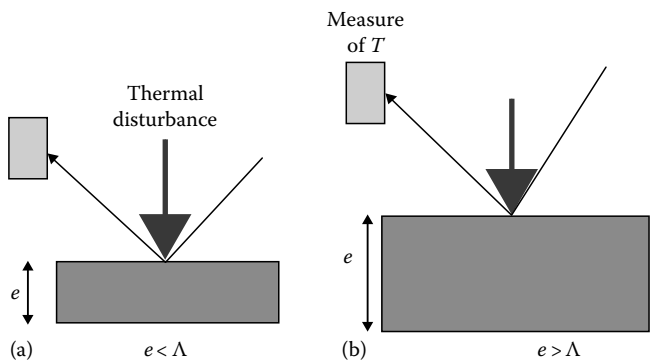

FIGURE 1.4
Thermal characterization using the front face experiment. (a) If the sample thickness e is less than the mean free path Λ of the heat carriers (electrons/phonons) the experiment allows identification of the thermal resistance (or conductance) of the layer only. (b) In the opposite case, the method allows identification of the thermal effusivity of the layer.

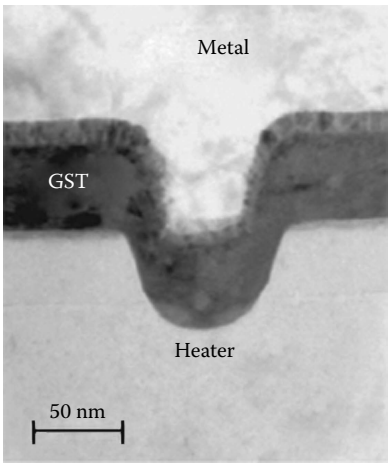

FIGURE 1.5
Nanoelectronics: a nonvolatile memory cell based on phase change chalcogenide alloy (GST stands for germanium–antimony–tellurium). The characteristic dimension of the cell is 50 nm.

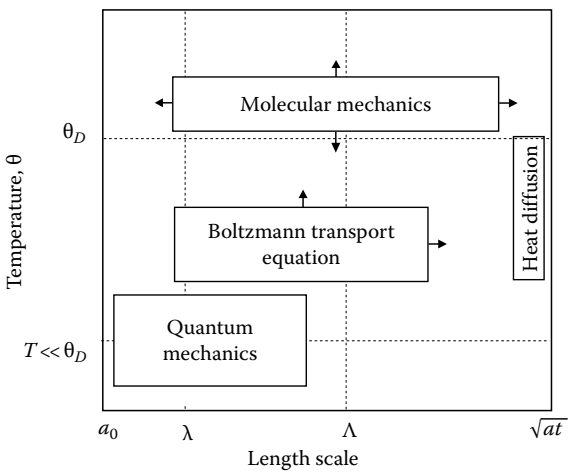

FIGURE 1.6
At dimensions comparable to the phonon wavelength λ and temperatures much smaller than the Debye temperature θ_D, heat transfer rests essentially on quantum mechanics. For larger dimensions and room temperatures, the BTE and the classical MD are well adapted for modeling heat transfer inside the studied structure. For even larger dimensions, Fourier's law can be efficiently implemented with a denoting thermal diffusivity.

specific tools that will be developed now. According to the scale, four types of methods will be used for constructing a heat transfer model, as described schematically in Figure 1.6.

We will first present the transport of heat through molecular dynamics (MD). We will then skip to Boltzmann transport equations (BTE) and present the two-temperature model further on. These models allow taking local thermal nonequilibrium into account. This nonequilibrium occurs between the thermal states of the electron gas and the crystal lattice, for metals and for semiconductors and only of the lattice for insulators. We will come finally to the model of heat diffusion designed by Fourier nearly 200 years ago. We will pinpoint, for each type of approach, the possibilities of measurement inversion. In other words, we will seek to define what are the physical parameters accessible to measurement and what are the thermal properties inherent to each.

1.2.3.2 Molecular Dynamics

MD aims at calculating the position, speed, and acceleration of ions or molecules that make up the material according to the classical Newtonians' mechanics equations, that is, the fundamental principle of dynamics (FPD). For a detailed description of the method, see the

book of Volz (2007) as well as that of Frenkel and Berend (1996). MD also leads to reliable results when quantum effects are predominant by using ab initio calculation starting from the Schrödinger relation. These quantum effects appear at low temperature and more precisely below Debye temperature. One will be able thus to use the FPD in MD only for $T > \Theta_D$. Another criterion to validate the use of FPD consists in calculating the ratio λ/a_0 where λ is the average wavelength of the ion (or molecule) vibration and a_0 is the interatomic distance. The relationship between wavelength λ, particle mass m, and temperature T is

$$\lambda = \frac{\hbar}{\sqrt{2\pi m k_B T}} \tag{1.9}$$

In this relation, $\hbar$ is Planck's constant and k_B is Boltzmann's constant. We note $\vec{r}_i$, $\vec{v}_i = \mathrm{d}\vec{r}_i/\mathrm{d}t$, and $\vec{a}_i = \mathrm{d}\vec{v}_i/\mathrm{d}t$ the position, speed, and acceleration of particle i, respectively. The total energy of particle i is the sum of its kinetic and potential energy:

$$E_i = E_{c_i} + E_{p_i} \tag{1.10}$$

The potential energy is itself the sum of an external potential field (such as an electromagnetic field) and of an internal field (caused by mutual interactions of the particles).

The force that is exerted on each particle thus derives from the potential energy:

$$\vec{F}_i = -\overrightarrow{\nabla} E_{p_i}(\vec{r}_i) \tag{1.11}$$

FPD applied to one particle is then

$$\vec{F}_i = m\vec{a}_i \tag{1.12}$$

Solving this vector-relationship (three scalar equations in three dimensions) for each particle (see Figure 1.7) leads to the position and then to the velocity of each particle. Calculation of its kinetic energy derives from knowledge of its speed:

$$E_{c_i} = \frac{m_i v_i^2}{2} \tag{1.13}$$

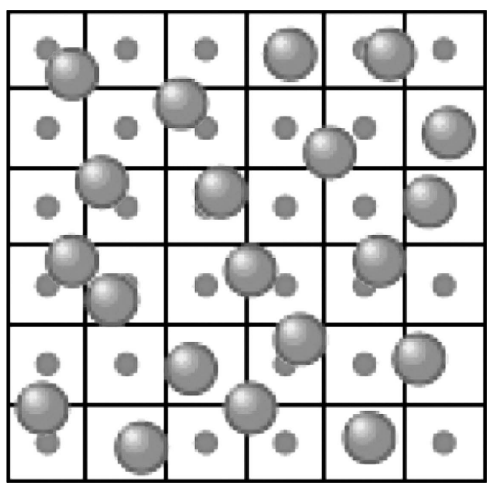

FIGURE 1.7
Classical configuration used for particle motion simulation using the MD. Periodic boundary conditions on the cell are generally assumed.

The kinetic theory provides temperature as follows:

$$T = \frac{2}{3k_B} E_{c_i} \tag{1.14}$$

Temperature is not subscripted by i deliberately because the notion of temperature relies on a large number of particles. Even if the mass of the particle is not present explicitly in the expression of temperature above, that is not true any more when various elements make up the material. In this case, one of the masses is taken as a reference and a mass correction is made for the other elements.

The theoretical difficulty in MD stems from the calculation of the potential of interaction between the particles.

MD can be implemented at the very low scale in order to calculate thermal conductivity of solids using non-homogeneous non-equilibrium molecular dynamics (NEMD) (see Figure 1.8). This is certainly the simplest technique (compared to the Green–Kubo calculation at equilibrium) to understand and implement, for it is analogous to the well-known guarded hot plate experiment. The idea is to simulate steady-state one-dimensional heat transfer in a system by inserting a hot and a cold source and then calculating the flux exchanged between the sources as well as the temperature gradient. The most widely used approach consists in adapting the velocity field of the atoms belonging to the heat sources in such a way as to impose the thermal power exchanged between the hot and cold sources. This method requires a large computation time: the number of particles that must be retained in this simulation is large since temperature is a statistical quantity.

Moreover, since thermal conductivity calculation requires defining a thermal gradient, the number of required particles increases dramatically in order to get a precise enough corresponding derivative. Moreover, this simulation always leads to the value of the thermal resistance R_{th} (the inverse of thermal conductance K defined in Section 1.2.3.1) of the material inserted between the hot and cold plates. This quantity is certainly as

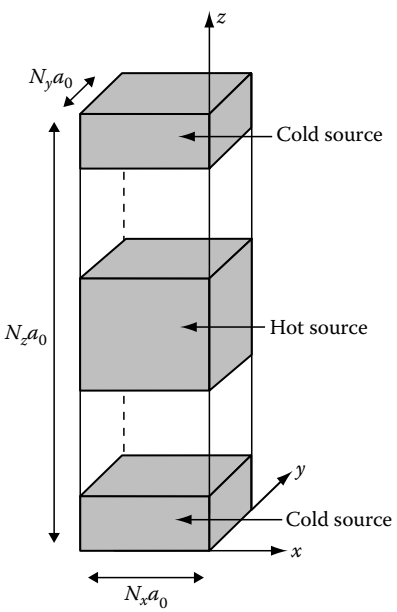

FIGURE 1.8
Nonequilibrium MD simulation for thermal conductivity simulation.

interesting as thermal conductivity in practical configurations encountered in engineering. As we said previously, if one wants to relate thermal resistance R_{th} to thermal conductivity k from the classical relationship $R_{th} = L/k$, then the dimension of the simulation box must be chosen as $L \gg \Lambda$, where Λ is the mean free path of the phonons.

We introduce now some basic ideas concerning the statistical nature of temperature since it is not always clear at very small scales. Using statistical mechanics arguments, temperature in a perfect gas can be defined for each particle of the gas. For liquids or solids, another definition, based on the interactions between the particles, must be given. Thus, the true question is the lowest size down to which the average energy of the phonons can be calculated. The answer is related to the value of the mean free path introduced in the preceding paragraph that is the distance separating two successive collisions of a phonon. If two areas in space have different temperatures, then they have also a different distribution of phonons. We know that this distribution can be modified only through the process of collisions. Anharmonic processes (processes where the assumption of small oscillations of particles around their equilibrium state is no longer valid) are responsible on thermal conductivity itself. The low frequency phonons have a large mean free path and correspond to low temperatures. In the so-called Casimir limit, for low temperatures, the mean free path size is about the same as the dimension of the material system. For high temperatures, on the contrary, phonons have a high frequency and mean free paths become much smaller. An illustration is given in Figure 1.9, where it is clearly demonstrated that the thermal conductivity and thus the temperature gradient take sense only when the number of particles involved in the MD simulation is high enough.

MD can be efficiently used as the direct model in an inverse procedure. Since inversion calls upon the model several times, it seems that it will take huge computational times. In order to answer the question about the parameters than can be estimated, it clearly appears that the unknown parameters in the model relate to the potential functions between each particle. Thus, one can imagine measuring the thermal conductance of a thin layer and then using this result as the minimizing function. To our knowledge, no work has ever been published on such a topic.

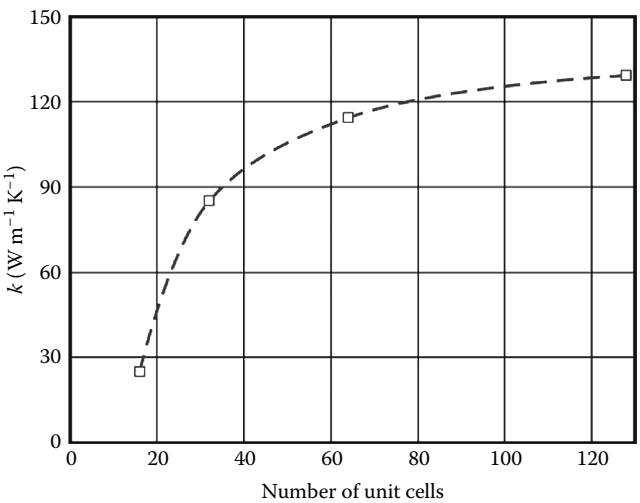

FIGURE 1.9
Result of NEMD simulation for silicon. Thermal conductivity is calculated according to the number of unit cells (crystal cell). As expected, thermal conductivity tends asymptotically toward the experimental value as the number of unit cell becomes high enough.

1.2.3.3 Boltzmann Transport Equation

The phonon BTE describes the rate of change of a statistical distribution function for phonons. The fundamental assumption in deriving the phonon BTE is that a distribution function, $N_q(\vec{r}, t)$, exists. It describes the average occupation of phonon mode q (this mode is associated with frequency ω_q and with wave vector $\vec{k}_q$ that are related through the dispersion curve for the studied material) in the neighborhood of a location $\vec{r}$ at time t. This equation relies on the assumption that phonon position and momentum can simultaneously be known with an arbitrary precision. However, in quantum mechanics, these quantities correspond to noncommuting operators and hence obey the uncertainty principle. The BTE is formally written as follows (see Volz [2007]):

$$\frac{\partial N_q(\vec{r}, t)}{\partial t} + \vec{v}_q \cdot \overrightarrow{\nabla} N_q(\vec{r}, t) = \left.\frac{\partial N_q(\vec{r}, t)}{\partial t}\right]_c \tag{1.15}$$

where $\vec{v}_q$ is the group velocity associated to phonon of wave vector $\vec{k}_q$. The term on the right-hand side is the rate of change due to collisions. Solution of the phonon BTE requires evaluation of the collision term, which constitutes the challenging problem here. The relaxation time approximation, associated with mode q, is widely used to model it. Under this approximation, the BTE is rewritten using the average distribution function $\overline{N}$ as follows:

$$\frac{\partial N_q(\vec{r}, t)}{\partial t} + \vec{v}_q \cdot \overrightarrow{\nabla} N_q(\vec{r}, t) = -\frac{N_q(\vec{r}, t) - \overline{N}}{\tau_q} \tag{1.16}$$

A key conceptual problem in using the relaxation time approximation is the requirement for a thermodynamic temperature that governs the scattering rate. Since phonons are not in an equilibrium distribution, there is no temperature to strictly speak of. The usual practice in such nonequilibrium problems is to define an ad hoc equivalent temperature based on the local energy.

The BTE can be efficiently used in order to compute the thermal conductivity of solids. Indeed, it is demonstrated that thermal conductivity can be related to thermal capacity c_v (J kg^{-1}) as follows:

$$k = \int_0^{q_{max}} v_q^2 c_v(q) \tau_q \, \mathrm{d}q \tag{1.17}$$

Specific heat can also be expressed analytically in terms of frequency mode ω_q and of temperature T as follows:

$$c_v(\omega_q) = \frac{3\hbar^2}{2\pi^2 k_B T^2 v_q} \int_0^{\omega_{max}} \frac{e^{\hbar\omega_q/k_B T}}{\left(e^{\hbar\omega_q/k_B T} - 1\right)^2} \omega_q^2 q^2 \, \mathrm{d}\omega_q \tag{1.18}$$

The frequency mode is related to the wave vector through the dispersion curves of the material. However, we must insist on the fact that this definition of thermal conductivity rests on the fact that the use of Fourier's law is allowed. In other words, time t must verify $t \gg t_c$, and characteristic dimension L of the medium must be such as $L \gg \Lambda$, in order to

define the temperature gradient inside the medium. These conditions are less restrictive for the definition of the specific heat since it only involves temperature and not its gradient.

The question now is as follows: does the BTE can be considered as the direct model in an inverse procedure and for identifying what? The answer is clearly yes since, as viewed previously, there is an analytical model for both specific heat and thermal conductivity. This model could be implemented in order to estimate the mean relaxation time of the phonons inside the material, which is generally unknown. Again, to our knowledge, such a work has not been made or published yet.

1.2.3.4 The Two-Temperature Model

We conclude this first part with the two-temperature model that constitutes a very good transition to homogenization methods at the macroscopic scale that will be described further on. The two-temperature model describes the time-dependent electron and lattice temperatures, T_e and T_l, respectively, in a metal or in a semiconductor during the thermalization process as follows:

$$c_e(T_e)\frac{\partial T_e}{\partial t} = \overrightarrow{\nabla} \cdot (k_e(T_e, T_l)\overrightarrow{\nabla} T_e) - G(T_e - T_l) + q_{vol} \tag{1.19}$$

$$c_l \frac{\partial T_l}{\partial t} = G(T_e - T_l) \tag{1.20}$$

In these equations, c_e and c_l are the electronic and lattice specific heat per unit volume, k_e is the electronic thermal conductivity that can be assimilated to bulk thermal conductivity for metals, and q_{vol} is the volumetric heat source in the lattice. These two nonlinear equations are coupled through the electron–phonon coupling constant G that can be explicitly defined starting from the BTE for both electrons and phonons. A detailed explanation of this model foundation can be found in the paper of Anisimov et al. (1974, 1975).

Regarding the TDTR reference experiment (see Section 1.2.2), Equation 1.19 means that, after the pulse, hot electrons will move inside the medium while losing their energy to the lattice. Let us insist on the fact that this model has a physical meaning only during the thermalization process, since Equation 1.20 shows that the lattice temperature remains constant as soon as $T_e = T_l$ or, in other words, when the thermalization process between electrons and lattice ends.

It must be also emphasized that this model involves a temperature gradient in the electron gas whereas thermal conduction in the lattice is neglected with respect to heat exchange between electrons and the lattice. It means that the characteristic length of the medium is such as $L \gg \Lambda_e$, where Λ_e is the mean free path of the electrons. Indeed, we saw previously that the mean free path for electrons is larger than for phonons. However, the constraint on time is just related to the relaxation time for electrons, which is of the order of some tenth of femtoseconds. In other words, the simulation time range for the two-temperature model can be (and should be) shorter than the relaxation time for the phonons.

When implementing the model in relation with the thermoreflectance experiment, the heat source q_{vol} is a function of the heated area (laser beam radius) of the optical penetration depth of the beam inside the material (related to the extinction coefficient) and of the intensity of the source.

We used the finite element method in order to simulate the two-temperature model starting from parameters given in the literature for aluminum. This simulation remains

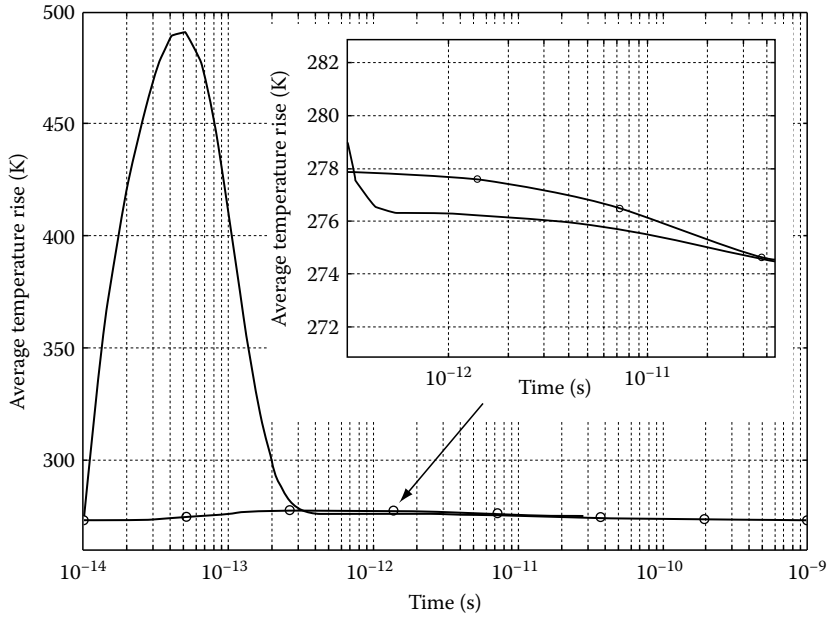

FIGURE 1.10
Two-temperature model simulation for the aluminum sample using the finite element method. Line with circles represents the lattice temperature; plain line is the electron gas temperature.

coherent with the definition of temperature for the electron gas and the lattice since the sample thickness has been chosen larger than the mean free path of the electrons in aluminum, which is approximately 10 nm (in other words, the minimum distance between two nodes of the mesh should be larger than this critical length). The resulting time-dependent temperatures of the lattice and of the electron gas are reported in Figure 1.10. The electron gas temperature increases very quickly and reaches its maximum at 50 fs. Temperature of the lattice begins to increase at 20 fs and reaches the electrons gas temperature at $t_c = 200$ fs. The calculation shows the undercooling of the electrons relative to the lattice at the surface. This undercooling comes from the high value of the coupling factor for aluminum. It is also observed for gold or copper whose coupling factors are smaller, but it is less pronounced than for aluminum. Figure 1.10 shows that complete thermalization between electron gas and lattice is reached at times between 25 and 30 ps. It demonstrates what was said in Section 1.2.2, that is, the relaxation time is lower than time t_c that has been estimated through the TDTR experiment.

The use of the two-temperature model as a model to invert has been made by Orlande et al. (1995) in order to estimate the coupling factor G for several kinds of metals. In fact, analytical expressions for this parameter are generally inaccurate: knowledge of the dispersion curve for the studied material is required. It is then interesting to estimate it directly from measurements similar to those given by the TDTR.

Our reference experiment shows that at the thermalization end, the TDTR measured response is only sensitive to the lattice cooling, which means that use of the classical one-temperature model becomes appropriate in order to describe heat diffusion inside the medium. Let us note that the two-temperature model degenerates naturally toward the one-temperature model when $t > t_c$.

1.3 Heat Diffusion Model for Heterogeneous Materials: The Volume Averaging Approach

1.3.1 Model at Local Scale

Thermal properties of heterogeneous materials are often determined experimentally by assuming the sample behaves macroscopically like a homogeneous medium. Therefore, the reliability of measurements depends heavily on the validity of the ''homogeneous medium'' assumption (see also Chapter 2 on the same subject). This is particularly true for measurements based on transient heat conduction. Let us consider now an elementary volume (a sample of the medium) whose configuration is representative of the material. Such a representative elementary volume (REV) is shown in Figure 1.11 for a medium constituted of two phases σ and β.

The shape of the REV is arbitrary but its size is not: if the REV is a sphere of diameter $D = 2r_0$, this diameter should be much smaller than the size of the whole system L: $D/L \ll 1$; this sphere constitutes a sample of the material and its diameter must be larger than the scale representative of the distribution of the two phases in space (an averaged distance l_β separating the ''grains'' of the discontinuous phase σ embedded in the continuous phase β in Figure 1.11, for example): $D/l_\beta \gg 1$. If the local structure of the material within this REV does not change too much when this sphere is moved anywhere in the whole medium, this medium can be homogenized.

One assumes here that Fourier's law is applicable for both phases at any point whose location is determined by its position vector $\vec{r}$ and for each time t. Thermal conductivities are denoted k_σ and k_β, and specific heat per unit volume is denoted $(\rho c_p)_\sigma$ and $(\rho c_p)_\beta$, for phases σ and β, respectively.

The heat transfer model at the local scale is as follows:

$$(\rho c_p)_\sigma \frac{\partial T_\sigma(\vec{r},t)}{\partial t} = \vec{\nabla} \cdot (k_\sigma \vec{\nabla} T_\sigma(\vec{r},t)) \quad \text{for } \vec{r} \text{ in the } \sigma\text{-phase} \tag{1.21}$$

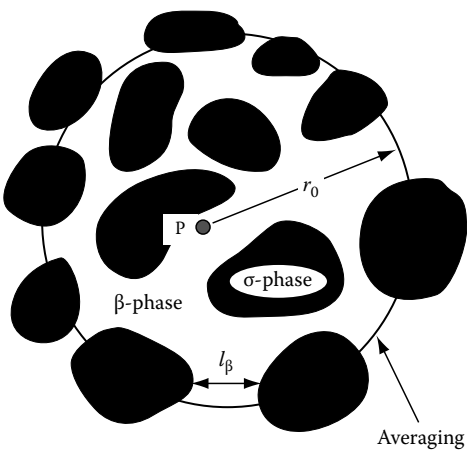

FIGURE 1.11
REV of a two-phase heterogeneous medium.

for the σ-phase, and

$$(\rho c_p)_\beta \frac{\partial T_\beta(\vec{r},t)}{\partial t} = \overrightarrow{\nabla} \cdot (k_\beta \overrightarrow{\nabla} T_\beta(\vec{r},t)) \quad \text{for } \vec{r} \text{ in the } \beta\text{-phase} \tag{1.22}$$

for the β-phase. Heat transfer between the two phases appears at the boundary condition at the σ–β interface.

Two homogenized models that transform this two-phase model into one single homogeneous (equivalent) phase can be now introduced. This homogenized medium may exist or not.

1.3.2 The One-Temperature Model

A volume averaging operator, noted $\langle\ \rangle$, can be defined here for any space field f at a point $\vec{r}$ located at the center $\vec{r}$ of the REV as follows:

$$\langle f \rangle(\vec{r},t) = \frac{1}{V(\vec{r},D)} \int_{V(\vec{r},D)} f(\vec{r}',t)\, \mathrm{d}V(\vec{r}') \tag{1.23}$$

where

$V(\vec{r},D)$, $\pi D^3/6$ here, is the volume of an REV centered at point $\vec{r}$

$\mathrm{d}V(\vec{r}')$ is a microscopic volume centered at any point $\vec{r}'$ located inside the REV

Thus, an averaged ''enthalpic'' temperature T_H can always be defined:

$$T_H(\vec{r},t) = \frac{1}{\langle \rho c_p \rangle V(\vec{r},D)} \int_{V(\mathrm{P},D)} \rho c(\vec{r}') T(\vec{r}',t)\, \mathrm{d}V(\vec{r}') = \frac{1}{\rho c_t} \langle H \rangle (\vec{r},t) \tag{1.24}$$

where $H(\vec{r},t)$ is the local enthalpy by unit volume: $H(\vec{r},t) = \rho c_t(\vec{r}) T_H(\vec{r},t)$, the total volumic heat ρc_t being defined by

$$\rho c_t(\vec{r}) = \langle \rho c_p \rangle(\vec{r}) = \varepsilon_\sigma (\rho c_p)_\sigma + \varepsilon_\beta (\rho c_p)_\beta \tag{1.25}$$

Here ε_σ and ε_β are the local volume fractions of the σ and β phases ($\varepsilon_\sigma + \varepsilon_\beta = 1$). These volume fractions are derived from the characteristic functions χ_α of each phase α (for $\alpha = \sigma$ or β), where $\chi_\alpha(\vec{r}) = 1$ if $\vec{r}$ belongs to the fluid phase and $\chi_\alpha(\vec{r}) = 0$ otherwise

$$\varepsilon_\beta(\vec{r}) = \langle \chi_\beta \rangle; \quad \varepsilon_\sigma(\vec{r}) = \langle \chi_\sigma \rangle = 1 - \varepsilon_\beta(\vec{r}) \tag{1.26}$$

One can notice that if the medium can be homogenized, its specific heat per unit volume ρc_t defined above should not depend on location $\vec{r}$.

The one-temperature model requires the definition of a thermal conductivity tensor $\overline{\overline{k}}$ whose coefficients can be considered as conductivities depending on the nature, thermophysical properties and geometry of the distribution of phases σ and β. A diffusion energy

equation for the space and time variations of the averaged temperature can be written in the case of a homogenized medium (Moyne et al., 2000):

$$\rho c_t \frac{\partial T_H}{\partial t} = \nabla \cdot (k \nabla T_H) + q_{vol} \tag{1.27}$$

where

q_{vol} is a volumetric source term

k is an effective (or equivalent) conductivity of the material that is supposed to be locally isotropic here (otherwise k has to be replaced by $\overline{\overline{k}}$)

This model can be extended to take fluid flow into account (see Testu et al. [2007]).

1.3.3 The Two-Temperature Model

At this stage, we introduce now the notion of intrinsic phase average, noted $\langle\,\rangle^{\alpha}$ here, for any time–space field $f(\vec{r},t)$ defined in the α-phase:

$$\langle f_\alpha \rangle^{\alpha}(\vec{r},t) = \frac{1}{V_\alpha(\vec{r},D)} \int\limits_{V_\alpha(\vec{r},D)} f(\vec{r}\,',t)\,\mathrm{d}V(\vec{r}\,') \quad \text{for } \alpha = \sigma \text{ or } \beta \tag{1.28}$$

where $V_\alpha(\vec{r},D) \subset V(\vec{r},D)$ designates the volume occupied by the α-phase ($\alpha = \sigma$ or β) in the REV shown in Figure 1.11. Subscript α of f_α indicates that integration is made for $\vec{r}\,'$ belonging to the $V_\alpha(\vec{r},D)$ volume, while superscript α, in $\langle\,\rangle^{\alpha}$, is related to division by volume $V_\alpha(\vec{r},D)$ in the right-hand member of this equation: $\langle . \rangle = \varepsilon_\alpha \langle . \rangle^{\alpha}$.

One can therefore introduce two different average temperatures $\langle T_\alpha \rangle^{\alpha}$ at the same point $\vec{r}$. These two temperatures are related to the previous averaged ''enthalpic'' temperature T_H through the definition of the average enthalpy:

$$\langle H \rangle = \rho c_t(\vec{r}) T_H = (\rho c_p)_\sigma \langle T_\sigma \rangle^{\sigma} + (\rho c_p)_\beta \langle T_\beta \rangle^{\beta} \tag{1.29}$$

In the case of local thermal equilibrium the temperatures both $\langle T_\alpha \rangle^{\alpha}$ are equal, which implies that they are also both equal to the average enthalpic temperature, because of the previous equation and of the definition of ρc_t: $\langle T_\sigma \rangle^{\sigma} = \langle T_\beta \rangle^{\beta} = T_H$. In the opposite case, the enthalpic temperature still exists but its observation is somewhat involved because a perfect temperature detector would provide a temperature that will be either close to $\langle T_\alpha \rangle^{\alpha}$ or to $\langle T_\beta \rangle^{\beta}$, depending on the quality of its coupling with either of each phase. In any case, the sensor temperature would be close to T_H, because, by definition, this temperature lies in between these two temperatures.

The macroscopic description of heat transfer in heterogeneous media by a single energy equation does not imply the assumption of local thermal equilibrium between the two phases. However, in order to get such an equilibrium, as described by Carbonell and Whitaker (1984), some criteria must be verified.

We use now the following notation: D denotes the characteristic dimension of the REV of volume V, $a_v = A_{\sigma-\beta}/V$ is its specific area, that is the ratio of the area of the interface $A_{\sigma-\beta}/V$ between the two phases by its volume, V_σ is the volume of the σ-phase, $\varepsilon = V_\sigma/V$ is its volume fraction, and L denotes the characteristic dimension of the heterogeneous medium.

Then time t must verify (see Carbonell and Whitaker [1984])

$$\frac{\varepsilon(\rho C_p)_\sigma D^2}{t}\left(\frac{1}{k_\sigma}+\frac{1}{k_\beta}\right)\ll 1 \quad \text{and} \quad \frac{(1-\varepsilon)(\rho C_p)_\beta D^2}{t}\left(\frac{1}{k_\sigma}+\frac{1}{k_\beta}\right)\ll 1 \tag{1.30}$$

And the characteristic dimension L of the REV must verify

$$\frac{\varepsilon k_\sigma D}{a_v L^2}\left(\frac{1}{k_\sigma}+\frac{1}{k_\beta}\right)\ll 1 \quad \text{and} \quad \frac{(1-\varepsilon) k_\beta D}{a_v L^2}\left(\frac{1}{k_\sigma}+\frac{1}{k_\beta}\right)\ll 1 \tag{1.31}$$

Obviously, another factor that can affect the assumption of local thermal equilibrium is the location of the considered point with respect to the heat source: equilibrium cannot occur in the vicinity of this source. Such a situation is met, for example, for front face heat pulse excitation of a multilayer slab made of layers of different thermophysical properties.

For situations in which local thermal equilibrium is not valid, models have been proposed based on the concept of two macroscopic continua. Intrinsic average temperatures for the σ-phase and the β-phase are denoted by $\langle T_\sigma(\vec{r},t)\rangle^\sigma$ and $\langle T_\beta(\vec{r},t)\rangle^\beta$, respectively (see Equation 1.28).

The pore-scale temperature deviation in the σ-phase is defined by

$$T_\sigma(\vec{r},t)=\langle T_\sigma(\vec{r},t)\rangle^\sigma+\tilde{T}_\sigma(\vec{r},t) \tag{1.32}$$

One can introduce this decomposition into the pore-scale equation for the σ-phase and then form the volume average in order to obtain the macroscopic equation. After extensive use of the averaging theorem, the following energy equation emerges for the σ-phase:

$$\varepsilon(\rho c_p)_\sigma\frac{\partial\langle T_\sigma\rangle^\sigma}{\partial t}=\nabla\cdot\left(\mathbf{K}_{\sigma\beta}\cdot\nabla\langle T_\beta\rangle^\beta+\mathbf{K}_{\sigma\sigma}\cdot\nabla\langle T_\sigma\rangle^\sigma\right)-a_v h\left(\langle T_\sigma\rangle^\sigma-\langle T_\beta\rangle^\beta\right) \tag{1.33}$$

Equivalently, the same procedure for the β-phase leads to

$$(1-\varepsilon)(\rho c_p)_\beta\frac{\partial\langle T_\beta\rangle^\beta}{\partial t}=\nabla\cdot\left(\mathbf{K}_{\beta\beta}\cdot\nabla\langle T_\beta\rangle^\beta+\mathbf{K}_{\beta\sigma}\cdot\nabla\langle T_\sigma\rangle^\sigma\right)-a_v h\left(\langle T_\beta\rangle^\beta-\langle T_\sigma\rangle^\sigma\right) \tag{1.34}$$

The macroscopic conductivity tensors $\mathbf{K}_{\beta\beta}, \mathbf{K}_{\beta\sigma}, \mathbf{K}_{\sigma\beta}, \mathbf{K}_{\sigma\sigma}$ and the volumetric exchange coefficient $a_v h$ are given by the solution of three closure problems that have to be solved over unit cells representative of the medium characteristics (see the paper of Quintard et al. [1997]).

Let us note that the previous one- or two-temperature models have been derived using the volume-averaging technique. The same kind of results can be set using the homogenization technique, where two different independent coordinate systems can be defined, one at the local scale and the other one at the mesoscopic scale. The interested reader can refer to Auriault and Ene (1994) for an example of practical application of this type of technique.

1.3.4 Application to a Stratified Medium

Here, we are interested by the macroscopic thermal behavior of a stratified medium subjected to a Dirichlet boundary condition, the flux being parallel to the strata (see Figure 1.12).

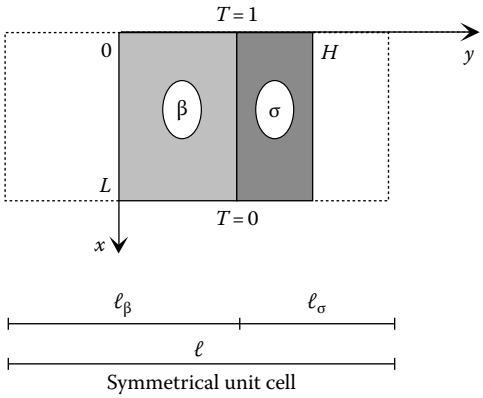

FIGURE 1.12
Stratified medium unit cell.

This choice is due to the fact that in this particular geometry, reference analytical exact solutions exist for the macroscopic effective properties, and only four effective parameters are independent and have to be identified.

Since the stratified medium is orthotropic and the main tensor axis coincides with the direction normal to the layers, the two-equation model is reduced to

$$\frac{\partial \langle T_\sigma \rangle^\sigma}{\partial t} = \frac{K_{\sigma\sigma}}{\varepsilon_\sigma (\rho c_p)_\sigma L^2} \frac{\partial^2}{\partial x^{*2}} \langle T_\sigma \rangle^\sigma - \frac{a_v h}{\varepsilon_\sigma (\rho c_p)_\sigma} \left(\langle T_\sigma \rangle^\sigma - \langle T_\beta \rangle^\beta \right) \tag{1.35}$$

and

$$\frac{\partial \langle T_\beta \rangle^\beta}{\partial t} = \frac{K_{\beta\beta}}{\varepsilon_\beta (\rho c_p)_\beta L^2} \frac{\partial^2}{\partial x^{*2}} \langle T_\beta \rangle^\beta - \frac{a_v h}{\varepsilon_\beta (\rho c_p)_\beta} \left(\langle T_\beta \rangle^\beta - \langle T_\sigma \rangle^\sigma \right) \tag{1.36}$$

where x^* is the dimensionless space variable x/L. Then, in this configuration, the four independent parameters to be identified are defined by

$$A_\beta = \frac{K_{\beta\beta}}{\varepsilon_\beta (\rho c_p)_\beta L^2}; \quad H_\beta = \frac{a_v h}{\varepsilon_\beta (\rho c_p)_\beta L^2}; \quad A_\beta = \frac{K_{\sigma\sigma}}{\varepsilon_\sigma (\rho c_p)_\sigma}; \quad H_\sigma = \frac{a_v h}{\varepsilon_\sigma (\rho c_p)_\sigma} \tag{1.37}$$

This study has been the subject of a paper of Gobbé et al. (1998).

1.4 Summary on the Notion of Temperature at Nanoscales and on Homogenization Techniques for Heat Transfer Description

We have seen above that in a solid material, temperature can be considered as a potential that ''explains'' transfer of energy and, at scales large enough, transfer of heat. At the nanoscale, its definition requires the presence of a high enough number of particles of each phase (ions in a lattice, electrons) because of its statistical nature. Once this condition is fulfilled, the studied medium can be considered as continuous, which means that any potential field or physical quantity can be assigned to any space point in the geometrical 3D Euclidian domain. Two different temperatures can be defined then, one for each phase, at

the same location. These can degenerate to one single temperature, if the two phases locally present at the same point reach equilibrium, depending on the time–space scales considered.

The same type of approach can be adopted at larger space scales, when solid materials composed of two phases are considered. At these larger scales, let us say above 10 nm, (1) the material is considered as continuous and (2) Fourier's law becomes valid at any point in space. Both previous conditions are not equivalent, since the second condition requires validity of the first one.

The use of an REV allows ''filtering'' the locally heterogeneous material, which leads to the definition of either one single ''average enthalpic temperature'' or two ''intrinsic average temperatures,'' verifying one or two coupled heat equations.

If the structure of the REV is not modified by its translation in space, the material can be considered as homogenous. Modification by rotation leads to anisotropic properties, but this notion does not derive from the spatial distribution of the two phases only. Under this condition of invariance by translation, the REV averaged thermophysical properties of the material become constant that is uniform in space. These properties are

- Its volume fractions ε_σ and ε_β defining its total volumetric heat ρc_t, and its effective thermal conductivity k (or a thermal conductivity tensor $\overline{\overline{k}}$ in the more general anisotropic case), for the one-temperature model (see Equation 1.29).
- The macroscopic thermal conductivity tensors $\mathbf{K}_{\beta\beta}, \mathbf{K}_{\beta\sigma}, \mathbf{K}_{\sigma\beta}, \mathbf{K}_{\sigma\sigma}$ and volumetric exchange coefficient, $a_v h$, for the two-temperature model (see Equations 1.35 and 1.36).

Homogenization techniques are presented in Chapter 2.

1.5 Physical System, Model, Direct and Inverse Problems

We will consider now on, in the presentation of inverse problems in heat transfer and in the remaining part of this chapter, the generic case of heat diffusion in an isotropic or anisotropic material that verifies the one-temperature model heat equation (based on Fourier's law), but its (continuous) material thermophysical properties (conductivity tensor $\overline{\overline{k}}$ and total volumic heat denoted ρc now) may vary in space (nonhomogeneous case) and possibly with temperature (thermodependent properties of the material).

1.5.1 Objective of a Model

The model-builder has a given objective: he tries to represent the real physical system by a model $\boldsymbol{M}$ that will be used to simulate its behavior. This model requires the knowledge of a given number of structural parameters that are put inside a parameter vector $\boldsymbol{\beta}$. Its objective is to get identical responses of both system $y(t)$ and model $y_{mo}(t, \boldsymbol{\beta}, u)$, under the excitation by an identical time-varying stimulus $u(t)$ (see Figure 1.13).

If the control science terminology is used, this stimulus is called « input » and the response « output ». These two terms have no geometrical meaning here.

In heat transfer, the stimulus is produced either by a source, that is, for example, a surface thermal power (absorption of a radiative incident flux by a solid wall, for example)

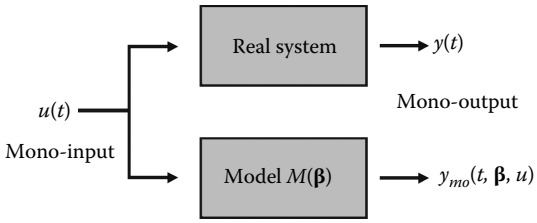

FIGURE 1.13
Real system and its representation by a model.

or by an internal power (Joule effect produced by an electrical current, heat of reaction of a chemical reaction,...). It can also be an imposed temperature difference (temperature difference between the inside and outside air environments on both sides of a solid wall, for example).

Let us note that if steady-state regime is considered, both stimulation u and responses y and y_{mo} do not vary with time.

1.5.2 State Model, Direct Problem, Internal and External Representations, Parameterizing

1.5.2.1 Example 1: Mono Input/Mono Output Case

Figure 1.14 shows a semi-infinite medium in the x-direction, whose front face ($x = 0$) is stimulated by a heat flux u (W m^{-2}) at initial time $t = 0$. The initial temperature distribution $T_0(x)$ may be nonuniform. A temperature sensor is embedded at a depth x_s inside the medium and delivers a signal y. So, starting at initial time, a transient 1D temperature field $T(x, t)$ develops inside the medium.

This temperature field, also called ''state'' of the system, is the solution of the heat equation, a partial derivative equation here, as well as of its associated boundary and initial conditions.

These equations are called *state equations* of this thermal system.

Different structural parameters appear in these equations: the medium heat conductivity k (W m^{-1} K^{-1}) and its thermal diffusivity $a = k/\rho c$ (m^2 s^{-1}), where ρ and c are its density (kg m^{-3}) and its specific heat (J kg^{-1} K^{-1}), respectively. The theoretical signal of the sensor y_{mo} (response of the model), caused by the medium stimulation u, is given by the *output equation*.

$$y_{mo}(t) = T(x_s, t) \tag{1.38}$$

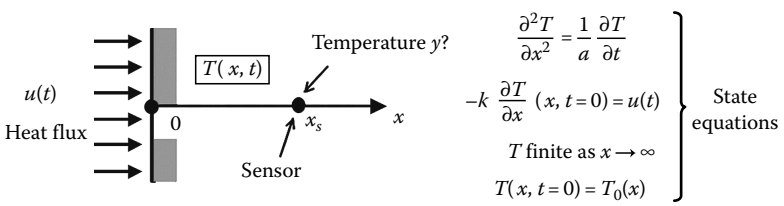

FIGURE 1.14
Model for the response of a temperature sensor embedded in a semi-infinite medium. The interrogation mark (?) designates what is looked for.

The state equations give an **internal representation** of the **direct problem** that allows the calculation of the system response everywhere, for a known excitation, while the sensor response is given by the output equation.

The state equations can be solved analytically here, and calculation of the output can be directly implemented, because the system is *causal*, *linear*, and invariant in time (see Ozisik [1980]):

$$y_{mo}(t) = \int_0^{\infty} G(x_s, x, t) T_0(x)\, \mathrm{d}x + \int_0^{t} Z(t-\tau) u(\tau)\, \mathrm{d}\tau = y_{mo\ relax}(t) + y_{mo\ forced}(t) \tag{1.39}$$

with

$$G(x_s, x, t) = \frac{1}{2\sqrt{\pi a t}} \left[\exp\left(-\frac{(x_s - x)^2}{4at} \right) + \exp\left(-\frac{(x_s + x)^2}{4at} \right) \right] \tag{1.40}$$

$$Z(t) = \frac{1}{b\sqrt{\pi t}} \exp\left(\frac{-x_s^2}{4at} \right) \tag{1.41}$$

where

- $G(x_s, x, t)$ is Green's function associated to relaxation, at location x_s, of the initial temperature field $T_{0(x)}$
- $Z(t)$ is the transfer function of the system, while $b = (k\rho c)^{1/2}$ is the thermal effusivity of the medium

Equation 1.39 indicates that two effects overlap: the first term corresponds to relaxation of the initial temperature field (free solution that vanishes for long times) while its second term, a convolution product, corresponds to the response (''forced'' solution) to the heat flux excitation. Transfer function Z that links a temperature response to an excitation power is called a time impedance, the same way as in AC electrical circuits. This function, once convoluted with the flux excitation u, yields the forced component of the temperature signal of the model. This can be expressed by a simple product of the corresponding Laplace transforms:

$$\bar{y}_{mo\ forced}(p) = \bar{Z}(p)\bar{u}(p) \quad \text{with } \bar{f}(p) = \int_0^{\infty} f(t) \exp(-pt)\, \mathrm{d}t \tag{1.42}$$

If initial temperature T_0 is uniform in the medium, the first term in $y_{mo}(t)$ in Equation 1.39 becomes equal to T_0.

This last equation constitutes an *external representation* of the direct problem. It makes calculation of the state $T(x, t)$ of the modeled system needless.

The (theoretical) output of the model depends on three parameters: the two thermophysical properties of the medium's material, a and b, and a parameter that relates to the sensor, that is, its location x_s. These three parameters can be gathered in a specific

parameter vector $\boldsymbol{\beta} = [a\ b\ x_s]^T$. This parameter vector $\boldsymbol{\beta}$ contains the structural parameters is of the problem: it does not change when input $u(t)$ and/or initial state $T_0(x)$ changes.

1.5.2.1.1 Important Point on Notation
Let us precise the notation that will be adopted now on

- A scalar or a scalar function depending continuously on an other scalar or vector variable (time t or temperature T, for example) will be noted in lower or upper case italic characters (k, or $T(t, x)$, for example).
- A column vector ($\boldsymbol{\beta}$, or $\boldsymbol{u}$, or $\boldsymbol{U}$ [see Equation 1.46] further down) or a column vector function will be noted in bold lower or upper case italic characters.
- A matrix or a matrix function will be noted in bold upper case characters (matrix $\boldsymbol{A}$ or matrix function $\boldsymbol{E}$ [see Equation 1.47] further down, except if this matrix function is a standard explicit function, such as the exponential of a matrix, noted **exp**(.) here).

The previous structural parameters $\boldsymbol{\beta}$, input u, and initial state T_0 can be assembled in a unique **list** (not a column vector made of scalar quantities here) of explanatory quantities $x = \{\boldsymbol{\beta}, u(t), T_0(x)\}$, gathering all the data necessary for the calculation of output y_{mo}.

Result of this modeling is sketched in Figure 1.15.

1.5.2.2 Parameterizing a Function

In the previous list x of explanatory quantities, one can find scalar parameters (diffusivity, lengths, ...) corresponding to structural parameters, as well as a time function $u(t)$, here a heat flux. Other functions can appear such as a nonuniform initial state $T_0(\mathrm{P})$ or a nonuniform structural parameter $\beta(\mathrm{P})$ or a parameter depending on temperature $\beta(T)$.

We suppose here that such a function is a time-depending input $x = u(t)$. In order to be able to deal with this kind of function, in the simulation (direct) problem and also in the inverse problem (finding u from measured y's, where this aspect becomes of prime importance), this function has to be parameterized by its projection on a selected basis of n chosen functions $f_j(t)$:

$$u_{param}(t) = \sum_{j=1}^{n} u_j f_j(t) \tag{1.43}$$

The new function u_{param}, replaced now by a vector $\mathbf{u} = [\,u_1 \quad u_2 \quad \cdots \quad u_n\,]^T$ of finite size n, is an approximation of the original u function that can consequently be considered as a vector with an infinite number of components. This approximation, that we will call **parameterization** now on, generates an a priori error that depends both on the chosen basis as well as on its size.

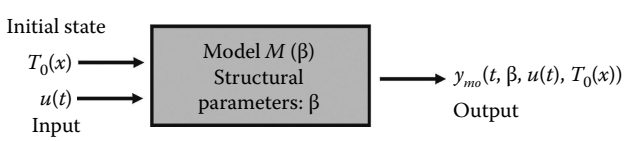

FIGURE 1.15
Input–output model for a thermal system.

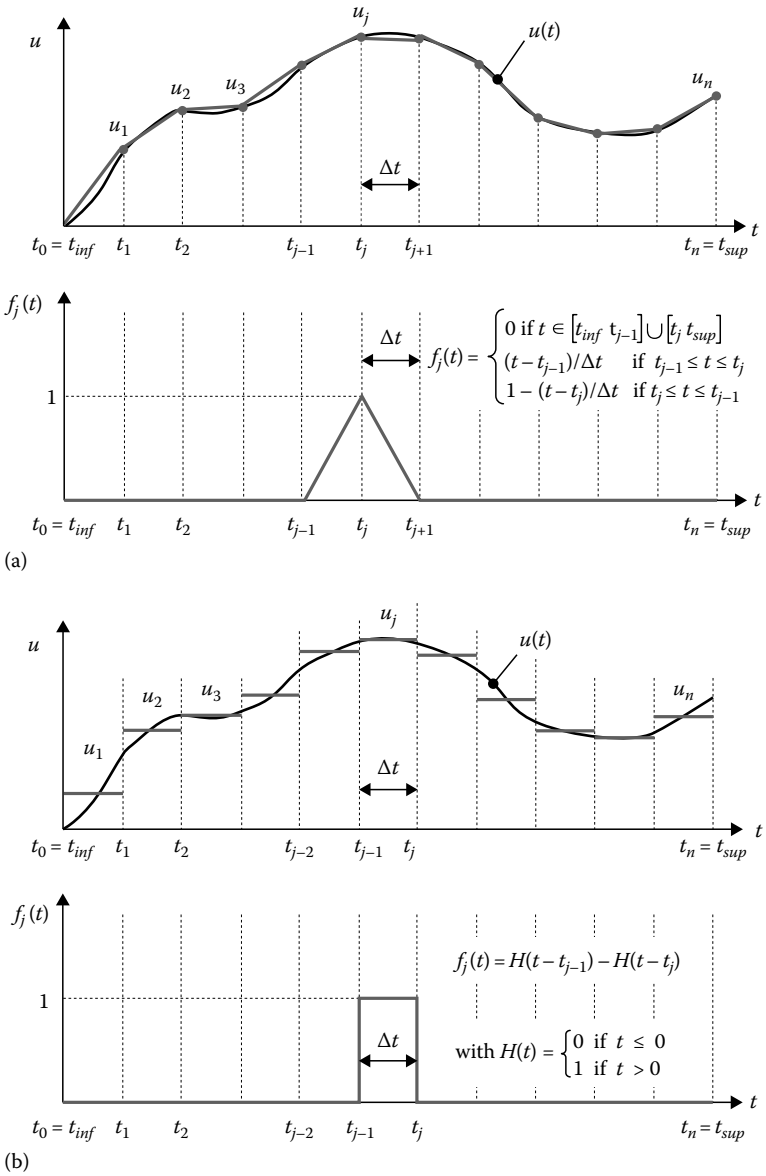

FIGURE 1.16
Two examples of function parameterization in a local basis: (a) parameterizing with a hat function basis and (b) parameterizing with a door function basis.

Figure 1.16 shows two possible choices, using a constant time step $\Delta t = t_j - t_{j-1}$:

- In case (a) the u_j components are the discrete values of the original function on the time grid and « hat » functions are selected as basis functions (see Figure 1.16a).
- In case (b) these components are averaged values of this function over one time step and « door » functions are selected for this basis (see Figure 1.16b).

The choice for the basis is not unique and strongly depends on the problem at stake.

So hat function *parameterization* of case (a) corresponds to linear interpolation using a table of discrete values; this parameterization choice is appropriate if a temperature dependency has to be modeled, for thermal conductivity $\lambda(T)$, for example. In that case, time t has to be replaced by temperature T in the basis functions that become $f_j(T)$.

In case (b), a piecewise constant function basis has been chosen. It suits deconvolution inverse problems, such as a time-varying source estimation using an experimental temperature response.

In both cases, each u_j component requires, for its calculation, knowledge of function $u(t)$ within the neighborhood of time t_j only. The use of such *local* bases is convenient because they directly derive from the time–space gridding. It is also possible to use projections on *nonlocal* bases such as polynomials, exponentials, trigonometric functions, etc.

The choice for a type of parameterization is very large. Constraints can be a priori set for the functions of the basis: they can present various properties such as monotony, regularity (continuous function with continuous first and second derivatives), and positivity, or they can be assigned fixed values on part of their time domain $[t_{inf}\ t_{sup}]$. One can also think of B-splines bases, wavelets bases....

Remark

The use of orthogonal function bases is possible: they correspond to functions $f_j(t)$ such as

$$\int_{t_{inf}}^{t_{sup}} f_j(t) f_k(t)\,\mathrm{d}t = N_j \delta_{jk} \tag{1.44}$$

where

δ_{jk} is Kronecker symbol ($\delta_{jk} = 0$ if $k \neq j$ and $\delta_{jk} = 1$ otherwise)

N_j is the square of the norm of function f_j

This kind of orthogonal projection, as well as its implementation, is deeply discussed in Chapter 14.

Door functions shown in Figure 1.16b are orthogonal, but it is not the case for hat functions shown in Figure 1.16a.

It is very interesting to choose the eigenfunctions of the heat equation (found using the method of separation of variables, see Ozisik [1980] for these f_j functions). In that case, the components of the corresponding $\boldsymbol{u}$ vector become integral transforms, that is, the different harmonics, of the original function (see the book *Thermal Quadrupoles*, by Maillet et al. [2000]). This method is related to singular value decomposition (see Press et al. [1992]).

1.5.2.3 State-Space Representation for the Heat Equation

The one-temperature heat equation can be written for a thermal diffusion problem in an anisotropic medium as the following partial differential equation:

$$\mathrm{div}\left(\overline{\overline{k}}\ \mathbf{grad}\ T\right) + q_{vol} = \rho c \frac{\partial T}{\partial t} + \text{Boundary, interface and initial conditions} \tag{1.45}$$

Here, q_{vol} designates the volumic heat sources (W m^{-3}) but other surface sources may be present in the boundary or interface conditions. $\overline{\overline{k}}$ designates the conductivity tensor here.

This partial differential equation system is of the evolution type and can be considered as a dynamical system. So, its solution, the temperature field $T(\mathrm{P}, t)$, that is, continuous in time, constitutes the state of the system, which can be noted here $T_{\mathrm{P}}(t)$, that is, for a given time t, a vector in an infinite dimension space.

This system that corresponds to a *distributed parameter system* can be discretized in space, using N nodes, the discretized state becoming a vector $T(t)$ in a N dimension space. The resulting state equation of this system takes the form of a *lumped parameter system* that corresponds to a system of first ordinary differential equations:

$$\frac{\mathrm{d}\boldsymbol{T}}{\mathrm{d}t} = \boldsymbol{E}(t, \boldsymbol{T}, \boldsymbol{U}) \quad \text{with } \boldsymbol{T}(t = t_0) = \boldsymbol{T}_0 \tag{1.46}$$

where vector $\boldsymbol{U}(t) = [u_1(t), u_2(t), \ldots, u_p(t)]^T$ corresponds to a local parameterization in space, but not in time, of the volumetric distributed source $q_{vol}(\mathrm{P}, t)$ and of the other sources possibly present in the boundary or interface conditions. The number of different parameterized sources is called p here.

Let us note that this equation is written here in the very general case of a fully nonlinear system where temperature is the only state variable: conductivity or volumetric heat may depend on temperature, or the associated interface/boundary conditions may not be linear (radiative surface heat losses, for example). In that case, matrix $\boldsymbol{E}$ depends on temperature $\boldsymbol{T}(t)$ in a nonlinear way. In a similar way, stimulation vector $\boldsymbol{U}$ may also be temperature dependent. In that case, each of the p components u_j of $\boldsymbol{U}$ is an implicit function of time, since it depends on the present and past states of the system, that is, on $\boldsymbol{T}$ on the $[0\ t_0]$ interval.

We assume to be in the linear case (linear heat equation system and linear source) now on

$$\boldsymbol{E}(t, \boldsymbol{T}, \boldsymbol{U}) = \boldsymbol{A}\boldsymbol{T} + \boldsymbol{B}\boldsymbol{U} \quad \text{with } \boldsymbol{A} \text{ and } \boldsymbol{B}\text{: constant matrices} \tag{1.47}$$

The different vectors and matrices present in the linear form of the state equation (1.47) are thus defined in Figure 1.17.

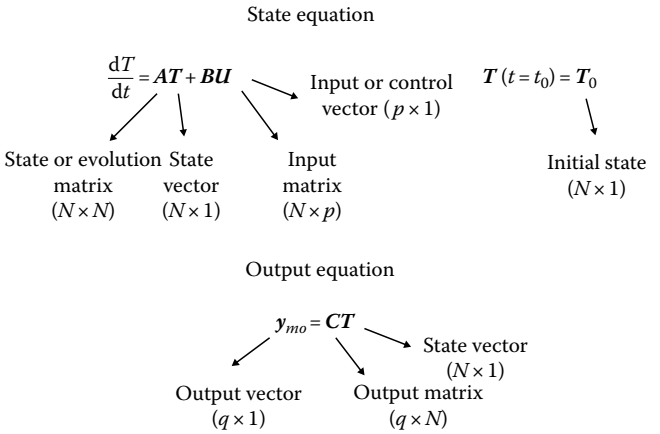

FIGURE 1.17
State and output equations for a linear dynamical thermal system.

An analytical solution for the state vector $\boldsymbol{T}(t)$ of this *state-space representation* of a linear system can be found formally using the exponential function of a matrix:

$$\boldsymbol{T}(t) = \mathbf{exp}(\boldsymbol{A}(t - t_0))\boldsymbol{T}_0 + \int_{t_0}^{t} \mathbf{exp}(\boldsymbol{A}(t - \tau))\boldsymbol{B}\boldsymbol{U}(\tau)\,\mathrm{d}\tau \tag{1.48}$$

In practice, and in the case of implementation of an inverse technique, all the N components of the state vector (temperatures at the different nodes of the model here) do not present the same interest: only a subset of it, composed of a selected number $q (q \leq N)$ of its components, constitutes the model output. They can correspond to observations provided by q sensors, for example. These outputs are numbered and called $y_{mo,i}$, and they are put in an *output vector* $\boldsymbol{y}_{mo}$:

$$\boldsymbol{y}_{mo} = \begin{bmatrix} y_{mo,1} & \cdots & y_{mo,i} & \cdots & y_{mo,q} \end{bmatrix}^T \tag{1.49}$$

Output vector $\boldsymbol{y}_{mo}$ is linked to state vector $\boldsymbol{T}$ through an output matrix (or observation matrix) $\boldsymbol{C}$, of $q \times N$ dimensions: the coefficients of this observation matrix are either 0 or 1's, according to the observed nodes:

$$\boldsymbol{y}_{mo} = \boldsymbol{C}\boldsymbol{T} \tag{1.50}$$

This equation is also called the *output equation*.

The response of the system, which is the observed output, can be calculated thanks to Equations 1.48 and 1.50 as

$$\boldsymbol{y}_{mo}(t) = \boldsymbol{C}\,\mathbf{exp}(\boldsymbol{A}(t - t_0))\boldsymbol{T}_0 + \boldsymbol{C}\int_{t_0}^{t} \mathbf{exp}(\boldsymbol{A}(t - \tau))\boldsymbol{B}\boldsymbol{U}(\tau)\,\mathrm{d}\tau \tag{1.51}$$

One notices, in a very similar way as in the previous example (1.39), that this response is the sum of a term corresponding to relaxation of initial state $\boldsymbol{T}_0$, which is the free regime, and a convolution product term corresponding to response to stimulation $\boldsymbol{U}(t)$, the forced regime.

The meaning of the notion of state appears clearly here: knowledge of the state of the system at a given time $\boldsymbol{T}(t_0)$ as well as the history of the different sources for the $[t_0\ t]$ time interval allows calculating the current state $\boldsymbol{T}(t)$ of the material system. So, at a given time, the thermal state contains the whole past of the system.

Remark 1.1

Equation 1.45 can easily be generalized to the case of heat transport in a pure fluid:

$$\begin{aligned} \mathrm{div}(\overline{\overline{k}}\ \mathbf{grad}\ T) - \rho c_f \boldsymbol{v} \cdot \mathbf{grad}\ T + q_{vol} &= \rho c \frac{\partial T}{\partial t} \\ &+ \text{boundary, interface, and initial conditions} \end{aligned} \tag{1.52}$$

where the advection term based on the volumetric heat of the fluid $\rho c_f = \rho c$ and on the fluid velocity $\boldsymbol{v}$ (solution of the Navier–Stokes and continuity equations) has been added and where, in this case, $\overline{\overline{k}}$ reduces simply to the thermal conductivity k of the fluid.

In the case of heat dispersion in a porous medium, this velocity has to be replaced by a local Darcy velocity, temperature T becomes an average ''enthalpic'' temperature at the local scale (for the one-temperature model), while $\overline{\overline{k}}$ becomes the thermal dispersion tensor, whose coefficients depend on this local Darcy velocity. In this case, ρc, the volumetric heat in the transient storage term, differs now from ρc_f. This total volumetric heat ρc results from a mixing law and represents the total volumetric heat of both fluid and solid phases, using the local volume fractions as weights (see Testu et al. [2007]).

Remark 1.2

State of a thermal system is not always composed of the sole temperature T. Two different examples of a composite state are given next.

If a physical or chemical transformation occurs inside the modeled material, a polymerization of a thermoset resin, for example, heat source is produced by the heat of reaction and usually depends on the degree of advancement of the reaction, through a kinetic law. This degree of advancement constitutes the second state variable. In that case, the state equations are composed of the heat diffusion Equation 1.45 completed with a coupled mass balance equation for each of the species present in the reacting system.

Another example can be given for coupled conduction and radiation heat transfer in semitransparent media. The radiative intensity is the second state variable, and the radiative transfer equation (an integro-differential of equation) will be associated with the heat diffusion equation in order to constitute the new state equations.

Remark 1.3

When a steady-state $\boldsymbol{T}_{ss}$ corresponding to an input vector $\boldsymbol{U}_{ss}$ exists, Equation 1.46 allows its calculation: it is written with $\mathrm{d}\boldsymbol{T}/\mathrm{d}t = 0$, which yields in the fully linear case (see Equations 1.46 and 1.47):

$$\boldsymbol{T}_{ss} = -\boldsymbol{A}^{-1}\boldsymbol{B}\boldsymbol{U}_{ss} \Rightarrow \boldsymbol{y}_{mo,ss} = -\boldsymbol{C}\boldsymbol{A}^{-1}\boldsymbol{B}\boldsymbol{U}_{ss} \tag{1.53}$$

1.5.2.4 Model Terminology and Structure

All the equations and necessary conditions for calculating the output of the model constitute the structure of the model, which can be written as a functional relationship, for a single output variable:

$$y_{mo} = \eta(t, x) \tag{1.54a}$$

or

$$y_{mo} = \eta(t, \boldsymbol{x}) \tag{1.54b}$$

where x is either a *list* (1.54a) of explanatory quantities, including functions, $x = \{\boldsymbol{\beta}, u(\mathrm{P}, t), T_0(\mathrm{P})\}$ or its vector version $\boldsymbol{x} = [\boldsymbol{\beta}\, \boldsymbol{U}\, \boldsymbol{T}_0]^T$ (1.54b), built with functions *parameterized* in space *and* time (or in temperature, for nonlinear problem with thermal

dependency of either input u or structural parameters β_j s). For output variables, one deals with an output vector (not a scalar y_{mo} anymore), which requires the use of a vector function $\boldsymbol{\eta}(.)$ whose arguments are time t and either the x list or its vector version $\boldsymbol{x}$:

$$\boldsymbol{y}_{mo} = \boldsymbol{\eta}(t, x) \tag{1.55a}$$

or

$$\boldsymbol{y}_{mo} = \boldsymbol{\eta}(t, \boldsymbol{x}) \tag{1.55b}$$

A wider meaning can be given for vector $\boldsymbol{U}$ in this last definition of parameter vector $\boldsymbol{x}$: this vector can represent, in a nonlinear case, a temperature-dependent stimulus $u(T)$ that has been parameterized. Let us note that a temperature-dependent thermophysical property $\beta_j(T)$, once parameterized, gives rise to constant coefficients of parameter vector $\boldsymbol{\beta}$. Coefficients of vector $\boldsymbol{\beta}$ can also stem from a space-dependent property $\beta_j(\mathrm{P})$ that has been parameterized in the case of a heterogeneous medium.

The ''direct problem'' consists in finding model output $y_{mo}(t; x)$ at a given time t in the $[t_0, t_{final}]$ interval, for known data $x = \{\boldsymbol{\beta}, u(\mathrm{P}, t), T_0(\mathrm{P})\}$. Solution of this problem can allow further numerical simulations of the output behavior.

A model relies on a given *structure*, that is, a functional relationship, noted η above, between the output variable (or explained or dependent variable) y_{mo} (an observed temperature here) and the independent variable (time t for transient problems) and a parameter vector $\boldsymbol{x}$, whose components are the parameterized explanatory quantities. It is important to remind that aside the previous structure, parameters $\boldsymbol{x}$ of the model should be defined accordingly (see Figure 1.18). They can either have a physical meaning if a state modeling is performed or simply a mathematical meaning without clear physical interpretation if an identified modelization is implemented.

One can notice that a model, in case of a single output, can provide not only a scalar output y_{mo} depending continuously on time t but also a vector output $\boldsymbol{y}_{mo}$. This output column vector $\boldsymbol{y}_{mo}$ is associated with the same output variable, a local temperature, for example, sampled at different times $t_1, t_2, \ldots, t_m$, or can result from a sampling of the explanatory variable that can be a space coordinate for a steady-state problem. It can

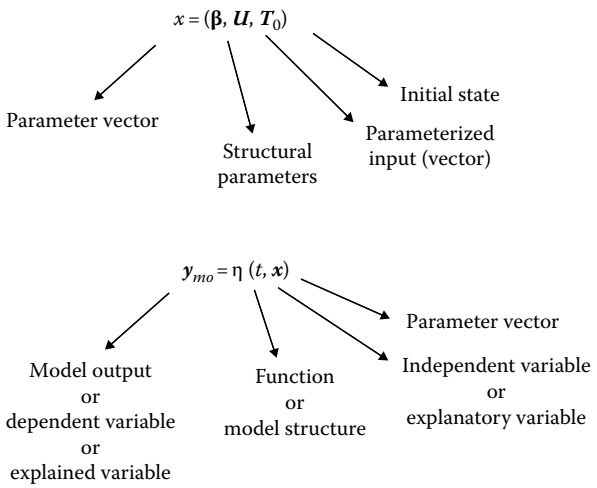

FIGURE 1.18
Parameter vector and structure of a model.

also gather in a single column vector, of length qm, several output temperatures observed at different points P_i ($i = 1$ to q), sampled for m different times t_k.

Let us note here that a general introduction to inverse problems is proposed in Chapter 7, and general methods and skills for their solution are discussed in Part II.

1.5.3 Direct and Inverse Problems

1.5.3.1 Direct Problem

We have seen above that when the studied problem allows it, the usual approach of the thermal science scientist consists in constructing a **knowledge-based model**, such as Equation 1.45, in order to be able to simulate the behavior of the physical system.

This leads to a numerical or analytical solution of a partial differential equation in the case of a heat diffusion problem (or an integro-differential system of equations for radiation heat transfer in semitransparent media, temperature, and radiative intensity being the state variables) that represents the corresponding transfer of heat. The solution of these equations also requires the knowledge of the conditions at the boundaries (Dirichlet, Neumann, Fourier, etc.) or at the internal interfaces (for a medium composed of different materials) as well as the initial condition in the system.

If an internal representation is adopted, several quantities of different nature have to be introduced in the state (1.45) and output equations $\boldsymbol{y}_{mo}(t) = T(P_i, t)$ of the model, written for a single temperature sensor located at point P_i. If the output is observed at q such points for m times that constitute a time vector $\boldsymbol{t} = [t_1\ t_2\ \cdots\ t_m]^T$, it becomes an output vector $\boldsymbol{y}_{mo}(\boldsymbol{t}; \boldsymbol{x})$ that depends also on parameter vector $\boldsymbol{x}$, where this vector is composed of

- The raw $u(P, t)$ or parameterized $\boldsymbol{U}(t)$ excitation
- Vector $\boldsymbol{\beta}_{struct}$ of structural parameters, a and b in Example 1 or coefficients of matrices $\boldsymbol{A}$ and $\boldsymbol{B}$ in the linear state equations (1.46) and (1.47)
- Vector $\boldsymbol{\beta}_{pos}$ describing the position of the observation, x_s in Example 1 and coefficients of matrix $\boldsymbol{C}$ in output equation (1.50)
- The initial temperature field $T_0(P)$ or its parameterized version $\boldsymbol{T}_0$

Input variables $u(P, t)$ are controlled by the user: they are either power sources or imposed temperature differences, inside or outside the system, that make temperature and output depart from a zero value in case of zero initial temperature $T_0(P)$.

Structural parameters $\boldsymbol{\beta}_{struct}$ characterize the system. They can be

- Geometrical quantities (shape and dimensions of the system)
- Thermophysical properties: conductivities, volumetric heat capacities, heat transfer coefficients, emissivities, contact or interface resistances, etc.

The relationship between output variables, generally a subset of the state, and state variables, the temperature field, makes the previous position parameter vector $\boldsymbol{\beta}_{pos}$ appear in this output equation.

A functional scheme corresponding to linear state and output heat equations is shown in the lower line of Figure 1.19.

This corresponds to the usual process of a model user: for a known initial state $\boldsymbol{T}(t_0)$, a known excitation $\boldsymbol{U}(t)$, and known structural parameters, the heat equation and the output

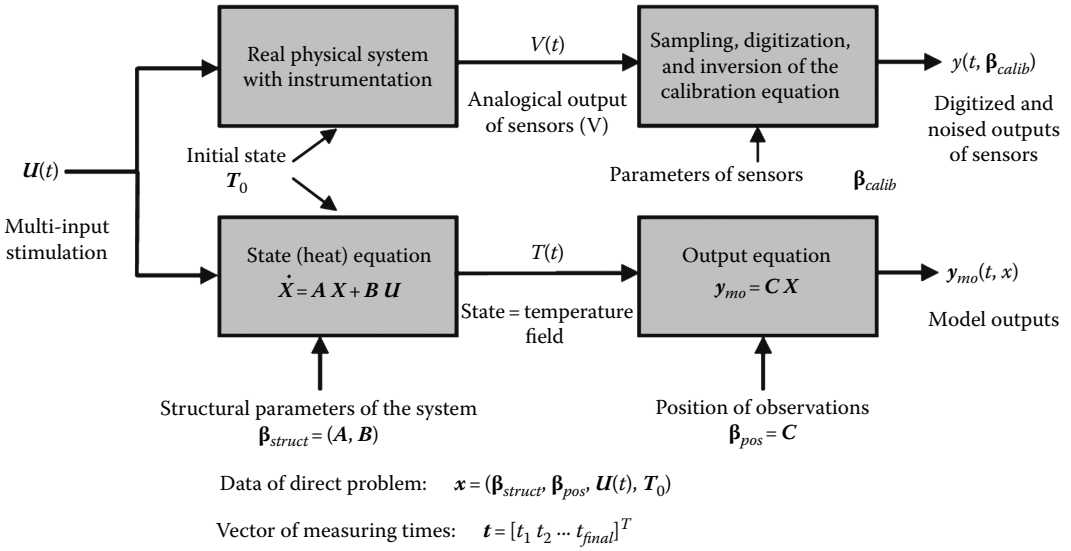

FIGURE 1.19
Linear model and material system with temperature measurement.

equations are solved sequentially to calculate the theoretical response $\boldsymbol{y}_{mo}$ of the sensors. This output corresponds to a possible real temperature measurement at the same locations (upper line in Figure 1.19). The **direct problem** can thus be solved.

1.5.3.2 Inverse Problem Approach

The preceding analysis shows that any variation in the data represented inside the $\boldsymbol{x}$ vector (including structural and position parameters $\boldsymbol{\beta}_{struct}$ and $\boldsymbol{\beta}_{pos}$) will produce a variation of the $\boldsymbol{y}_{mo}$ output.

Conversely, any variation of this output $\boldsymbol{y}_{mo}$ is necessarily caused by variation of some data inside $\boldsymbol{x}$.

The inverse approach is based on this principle. When knowledge of part of the variables that are necessary to solve the direct problem is lacking, data vector $\boldsymbol{x}$ of this problem can be split into two vectors the following way:

$$\boldsymbol{x} = \begin{bmatrix} \boldsymbol{x}_r \\ \boldsymbol{x}_c \end{bmatrix} \tag{1.56}$$

where

$\boldsymbol{x}_r$ now represents the (column) vector gathering the unknown part of the data that are *sought* (*researched*)

$\boldsymbol{x}_c$ is its *complementary* part that contains *known* data

In that case, solving the direct problem constitutes an impossible task. Any process aimed at finding $\boldsymbol{x}_r$ requires some *additional information*.

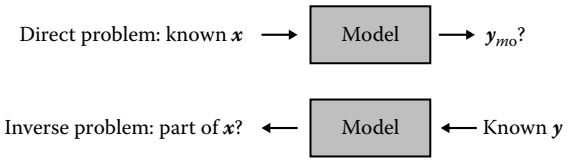

FIGURE 1.20
Direct problem/inverse problem. The interrogation mark (?) designates what is looked for in each problem.

Problems whose objective is to find a value for $\boldsymbol{x}$, starting from additional information, are called *inverse problems*.

Any inverse problem consists in making the model work in the « backwards » way: if outputs $\boldsymbol{y}$ as well as model structure η are known, part $\boldsymbol{x}_r$ of $\boldsymbol{x}$ will be sought, its complementary part being known (see Figure 1.20).

A general introduction to inverse problems is proposed in Chapter 7, and general methods and skills are discussed further in Sections 7.2 and 7.3 of the same chapter.

1.5.3.3 Inverse Problems in Heat Transfer

1.5.3.3.1 Different Types of Inverse Problems in Heat Transfer

The nature of additional information necessary for solving the inverse problem allows bringing out three main types of problems:

1. *Inverse measurement problems*, where this information stems from output signal $\boldsymbol{y}$ of sensors.
2. *Control problems*, where the previous measurements are replaced by desired values of either the state $T(\mathrm{P}, t)$ or output variables $\boldsymbol{y}$: data or $\boldsymbol{y}$ are the targets. In this class of problem, the sought quantity is generally the stimulus $u(\mathrm{P}, t)$ or the initial state $T_0(\mathrm{P})$, but it can also be a structural parameter (a velocity or a flow rate in a forced convection cooling problem, for example). In this class of problems, it is not always possible to reach the targets, for physical or mathematical reasons, and it may be necessary to specify a certain number of constraints on the sought solution.
3. *System identification problems*, that is, model construction for simulating the behavior of a system (see Chapters 13 and 14). These can be classified into two categories:
   a. *Model reduction*: $\boldsymbol{y}$ is the output of a detailed model $\eta_{det}(t; \boldsymbol{x}_{det})$ completely known, and the structural parameters (part of $\boldsymbol{x}_{red}$) of a reduced model $\eta_{red}(t; \boldsymbol{x}_{red})$ of given structure η_{red} are sought, both models sharing either identical or close stimulations $u(\mathrm{P}, t)$ and initial state $T_0(\mathrm{P})$ that are parts of $\boldsymbol{x}_{det}$ and $\boldsymbol{x}_{red}$. This can be written as follows:

$$\begin{aligned} \eta_{det}(t; \boldsymbol{x}_{det}) \approx \eta_{red}(t; \boldsymbol{x}_{red}) \quad \text{where } \boldsymbol{x}_{det} &= [\boldsymbol{\beta}_{det} \quad \boldsymbol{U}_{det} \quad \boldsymbol{T}_{0\,det}]^T \\ \text{and} \quad \boldsymbol{x}_{red} &= [\boldsymbol{\beta}_{red} \quad \boldsymbol{U}_{red} \quad \boldsymbol{T}_{0\,red}]^T \end{aligned} \tag{1.57}$$

with, for mathematical reduction:

$$\begin{aligned} u_{red}(\mathrm{P}, t) = u_{det}(\mathrm{P}, t) &\Rightarrow \boldsymbol{U}_{red} = \boldsymbol{U}_{det} \\ T_{0\,red}(\mathrm{P}, t) = T_{0\,det}(\mathrm{P}, t) &\Rightarrow \boldsymbol{T}_{0\,det} = \boldsymbol{T}_{0\,red} \end{aligned} \tag{1.58}$$

or, for physical reduction:

$$\begin{aligned} u_{red}(\mathrm{P},t) \approx u_{det}(\mathrm{P},t) &\Rightarrow \boldsymbol{U}_{red} = f_U(\boldsymbol{U}_{det}) \\ T_{0\,red}(\mathrm{P},t) \approx T_{0\,det}(\mathrm{P},t) &\Rightarrow \boldsymbol{T}_{0\,red} = f_{T\,0}(\boldsymbol{T}_{0\,det}) \end{aligned} \tag{1.59}$$

In both cases, *mathematical* or *physical model reduction*, the structural parameters of the reduced model depend on the corresponding parameters of the detailed model:

$$\boldsymbol{\beta}_{red} = f_\alpha(\boldsymbol{\beta}_{det}) \quad \text{for } \alpha = u \text{ or } T_0 \tag{1.60}$$

but this relationship, function f_α, is explicit for physical reduction (see Section 1.6), while it is not generally the case for mathematical reduction.

b. *Experimental model identification*: $\boldsymbol{y}$, $\boldsymbol{U}$, and $\boldsymbol{T}_0$ are measured, or supposed to be known, and the structural parameters (part of $\boldsymbol{x}$) of a model $\eta(t;\boldsymbol{x})$ of given structure η are known, $\boldsymbol{U}$ and $\boldsymbol{T}_0$ being their complementary part in $\boldsymbol{x}$.

Let us note that system identification leads to models that can be of the *white box* type, which means models based on first principles, for example, a model for a physical process from the Newton's equations. The previous state-space model (1.46), based on a heat balance and on Fourier's law defining heat flux, belongs to this category. The nature of the parameters in this class of models is perfectly known, which explains why they are used for thermophysical property estimation. Conversely, an identified model on an experimental basis, without a priori information on its structure, is also called a *black box* model: parameters of such a model have only a mathematical, but not physical, meaning. Such black box models may, for example, derive from neural network modeling. In between, one can find *gray box* or *semi-physical* models: the model, that is, the structure/parameter couple, is chosen according to a certain physical insight on what is happening inside the system, and these parameters are estimated on an experimental basis.

1.5.3.3.2 Inverse Measurement Problems in Heat Transfer

We will now focus on *inverse measurement problems* where model structure (the equations) η is known and where measurements $y(t)$ are available on the time interval $[t_0, t_{final}]$.

According to the nature of the explanatory variables $\boldsymbol{x}_r$ that are sought, solution finding for inverse problems may differ. One can distinguish in particular

1. Inverse problems of *structural parameters estimation*: $\boldsymbol{x}_r \equiv \boldsymbol{\beta}_r$
   System identification problems, of the black or gray box type, belong to this category: structural parameters (part of $\boldsymbol{x}$) of an ad hoc $\eta(t;\boldsymbol{x})$ model are sought through experimental characterization. *Thermophysical property estimation* belongs to the white box category: *intrinsic* parameters, that is, parameters that can be used for completely different simulation/experimental configurations are sought through experimental characterization. In both types of problems, several experiments on the same setup, for the same sample, can be repeated in order to estimate the same unknown parameter(s).
2. Inverse *input* problems: $\boldsymbol{x}_r \equiv u(\mathrm{P},t)$
   In heat transfer, this type of problem consists in finding the locations and values of the sources. Such a source, or excitation, is either a volumetric, surface, line, or

point heat source or simply a temperature difference imposed inside or at the boundaries of the system. It differs from the previous problem because the solutions sought are specific to each experiment made.

3. Inverse *initial state* problem: $\boldsymbol{x}_r \equiv T_0(\mathrm{P})$
   This problem is very close to the inverse input problem, since each sought solution is relative to a single given experiment.
4. Inverse *shape reconstruction* problems
   In the previous types of inverse problems, boundaries of the domain are usually fixed and known. In certain cases (problems with change of phase, in welding or in solidification applications, for example) shape of the domain (its boundary) or location of an interface between sub-domains (a change of phase moving front, for example) has to be taken into account in the variables defining the direct problem. In the corresponding inverse problem, the shape of this boundary has to be first parameterized in order to reconstruct it through inversion.
5. Inverse problems of *optimal design/control*
   A usual process aimed at reducing estimation errors, in a characterization process of type (1), consists in coupling it to an optimal conception/control problem for the characterization experiment. This optimization allows the design and the sizing of the experimental setup as well as the procedure for the trials that will bring additional information necessary for this characterization. This approach can provide a methodology for a pertinent choice of inputs, locations of measurement points, time observation windows, etc. The choice of these design quantities can be made in order to maximize a criterion based on the sensitivity of the output observations to the parameters that are sought. In heat transfer, characterization problems (that are structural parameter estimation or system identification problems) are usually nonlinear, which means that optimization of any design has to be implemented on the prior assumption that the sought parameters are known, with an iterative approach, once a first estimation has been found. This means that *nominal* values of these parameters are necessary for such a design.

Remark

The use of any sensor that very often delivers an electrical output quantity (a tension V, for example) requires the construction of a relationship between the quantity one wants to measure, temperature T here, and this instrument output.

It is therefore necessary to find, on the basis of the physical principle the sensor and the whole instrumental chain rely on, a model structure V_{mo} (T; $\boldsymbol{\beta}_{calib}$) where temperature is now the explanatory variable and where vector $\boldsymbol{\beta}_{calib}$ gathers all the parameters required for calculating the theoretical output temperature signal (thermoelectric power and cold junction temperature, in the case of a thermocouple sensor). Construction of the V_{mo} model and estimation of parameters present in $\boldsymbol{\beta}_{calib}$ starting from simultaneous measurements of both V and T (using a reference temperature sensor) constitute a *calibration problem*, that is, by nature, a parameter estimation problem, that is a type (1) inverse problem (see section above) that has to be dealt with this way.

1.5.3.4 Measurement and Noise

In *inverse measurements problems*, the additional information is brought by the measured output that differs from the model output y_{mo}.

The difference $\varepsilon(t)$ between a sensor measurement y and the output of an ideal sensor y^* giving the true temperature at the sensor location can be introduced:

$$y(t) = y^*(t) + \varepsilon(t) \tag{1.61}$$

The sensor giving y^* is ideal for two reasons: (1) its presence does not affect the local temperature of the medium (*non-intrusive* detector) and (2) it provides the *true value* of its *own* temperature.

Equation 1.61 defines the measurement noise $\varepsilon(t)$ that can be considered as a random variable caused by the imperfect character of both instrumentation and of digitization of the signal. This noise is present, but its deterministic value can not be reached in practice.

This equation also shows that the measured signal is a random variable whose variance is the same as noise ε.

The assumption of a pertinent, that is, non-biased, model is made in practice:

$$y^*(t) = y_{mo}(t, \boldsymbol{x}^*) \tag{1.62}$$

where $\boldsymbol{x}^*$ is the true value of the explanatory variables.

Verifying this assumption of consistency between model and measurements is crucial. Corresponding tools exist (study of the residuals).

Remark

Form (1.61) should be defined for discrete values $y_i = y(t_i)$, $\varepsilon_i = \varepsilon(t_i)$, and $y_i^* = y^*(t_i)$ corresponding to the sampling times t_i of the measured signal, of the exact temperature, and of the noise, respectively.

1.6 Choice of a Model

1.6.1 Objectives, Structure, Consistency, Complexity, and Parsimony

Before constructing a model, the model-builder has to be clear about the way his model will be used, that is, about the objective of such a modeling. The objectives depend on the application and can belong to one of the following categories that can be listed in a non-limitative way:

- Estimation of thermophysical properties
- Heat source/flux estimation
- Initial temperature field estimation
- Defect detection and nondestructive testing
- Simulation of the system behavior for better design or future state forecasting
- Model reduction for faster computation or use for heat source/flux estimation
- Conception of a model for closed-loop (feedback) control

So the type of model will not be the same for each application, because the required model precision will differ: defect detection in a composite slab using infrared thermography (Maillet et al., 1993) does not require a model with the same temperature resolution as in thermophysical property estimation, such as the flash method for liquid diffusivity estimation (Rémy and Degiovanni, 2005).

The accuracy of a model is determined by its consistency with the physical situation modelized, that is, its ability to simulate closely the behavior of the studied system. *Internal representation*, with the use of state-space models, should be generally favored, because it provides a mathematical structure linked to the physics of the modeled problem « for free ». In addition, this type of representation allows highlighting the intrinsic parameters of the system, that is, its thermophysical properties or thermal resistances and impedances.

The purpose of the model that is used for inverting measurements is not to reproduce or to mimic the whole temperature field: it should only provide an output that can be compared to the sensor output signal at the *location* where this one is embedded. Structure, that is, scalar or vector function η used above, is what defines a model. Its complexity should be adapted to the uncertainties associated with any description of a physical system: the use of a model that is too much simplified (simple structure with a low number of structural parameters, such as a *lumped parameter* model see Section 1.6.2) can introduce a systematic error, a bias, in its output variables, that could depart too much from model predictions and from the experimental observations to be used the inverse way. Conversely, the choice of a too-*detailed* model, with a high number of parameters

- Tends to make implementation of the inversion algorithm involved or to make it numerically impossible or very difficult.
- May lead to unstable solutions for the inverse problem, because of noise amplification (in case of inversion of measurements): the inverse problem becomes ill-posed.

This dilemma pleads in favor of the purpose of *parsimonious* models for inverse use, that is, models that provide a good balance between antagonist criteria of the use of a minimum number of parameters on the one hand and maximum agreement with reality (fidelity to measurements) on the other hand.

Up-to-date capacities of numerical simulation tools as well as structure of the *optimization* and *regularization* algorithms allow solving inverse problems with more and more complex models, using *mathematical model reduction* techniques. These allow a very significant reduction of the size of the state vector (temperature at different nodes of the numerical grid here). So reduction of a model, followed by its implementation in an inverse procedure, can bring an efficient approach for the most difficult cases, such as 3D heat transfer with change of phase or advecto-diffusive transfers within flowing fluids, for example (Girault et al., 2008). We will now focus on a different type of reduction technique, *physical model reduction*.

1.6.2 Example 2: Physical Model Reduction

In order to show that a thermal model can be reduced on a physical basis and that many models of different complexity and resolution are available to simulate the same heat

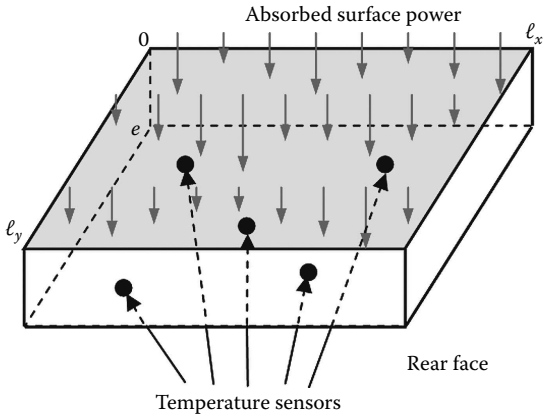

FIGURE 1.21
Model for temperature response of a slab heated on one of its faces.

transfer situation (nonuniqueness of a model), we will consider heat transfer in a slab, whose characteristics are defined as follows:

- Homogeneous rectangular slab, thickness e, lengths ℓ_x and ℓ_y in its plane
- Thermal diffusivity and conductivity a and k, respectively, volumetric heat $\rho c = k/a$

This slab is stimulated by a surface power (absorption of solar radiation, for example) on its front face, and temperature is measured at q points by sensors either embedded in the material or located on the front or rear face of the slab (see Figure 1.21). The slab is supposed to be insulated on its four (lateral) sides and exchanges heat with the surrounding environment T_∞ only on its rear face through a uniform heat transfer coefficient h that represents its losses (convection and linearized radiative losses). Its initial temperature T_0, at time $t = 0$, when heating starts, is supposed to be uniform.

A model allowing to find the temperature response $y_{mo,i}(t)$ of sensor number i ($i = 1$ to q) at time t is sought.

1.6.2.1 3D Model

Heat source $u(x, y, t)$ (W m^{-2}) is supposed to be nonuniform at the front face. Evolution with time of the temperature field can be described by a three-dimension transient model (see Figure 1.22a):

$$\frac{\partial^2 T}{\partial x^2} + \frac{\partial^2 T}{\partial y^2} + \frac{\partial^2 T}{\partial z^2} = \frac{1}{a}\frac{\partial T}{\partial t} \tag{1.63}$$

$$T = T_0 \quad \text{for } t = 0 \tag{1.64}$$

$$\frac{\partial T}{\partial x} = 0 \quad \text{at } x = 0, \ell_x; \quad \frac{\partial T}{\partial y} = 0 \quad \text{at } y = 0, \ell_y \tag{1.65}$$

$$-k\frac{\partial T}{\partial z} = u(x, y, t) \quad \text{at } z = 0; \quad -k\frac{\partial T}{\partial z} = h(T - T_\infty) \quad \text{at } z = e \tag{1.66}$$

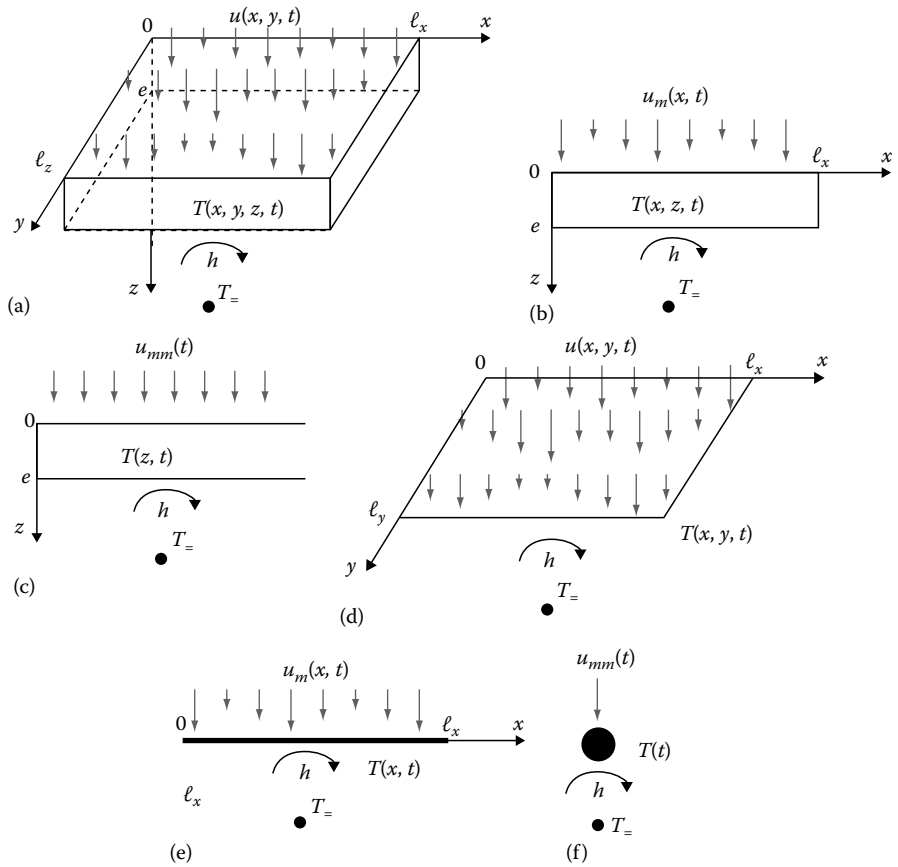

FIGURE 1.22
''Physical'' model reduction. (a) 3D model, (b) 2D model, (c) 1D model, (d) 2D fin model, (e) 1D fin model, (f) 0D lumped model: « small » body.

This system of eight equations constitutes model $\boldsymbol{M_a}$ that will be called ''detailed model'', whose solution, noted $T = T_a$ here, determines the response of each sensor:

$$y_{mo,\,i} = \eta_i(t, x) = T_a(x_i, y_i, z_i, t; u(x, y, t), T_0, T_\infty, h, \ell_x, \ell_y, e, \lambda, a) \tag{1.67}$$

In this equation, u, T_0, and T_∞ are input quantities of the model, independent from the structure of the material system (if they are all equal to zero, temperature stays to a zero level everywhere in the slab), while the other quantities are the structural parameters β, either linked to geometry (ℓ_x, ℓ_y, e), or to the thermophysical properties (k, a) of the slab material and to its coupling with the outside environment (h), or linked to the location of the sensors (x_i, y_i, z_i, for $i = 1$ to q).

List $x = \{\boldsymbol{\beta}, u, T_0, T_\infty\}$ can be introduced now. It gathers *structural parameters* $\boldsymbol{\beta}$, *inputs* u and T_∞, and initial state T_0 of this dynamical system composed of $(3q + 9)$ quantities.

1.6.2.1.1 Dimensionless 3D Model

The number of quantities present in Equations 1.63 to 1.66 can be reduced if they are written in a dimensionless form: dimensionless temperature $T^* = (T - T_\infty)/\Delta T$ appears,

with $\Delta T = T_0 - T_\infty$, and it is the same for dimensionless time, Fourier number $t^* = t/\tau_{diff}$, and dimensionless heat transfer coefficient, Biot number $H = he/k$. In a similar way, dimensionless observation locations $x_i^* = x_i/e$, $y_i^* = y_i/e$, $z_i^* = z_i/e$ and dimensions $\ell_x^* = \ell_x/e$ and $\ell_y^* = \ell_y/e$ are introduced.

Here, $\tau_{diff} = e^2/a$ is the characteristic time, related to the duration of thermal diffusion in the thickness of the slab. The resistance of the slab in the thickness direction, related to a unit area, $R = e/k$, can be introduced.

This new model $\boldsymbol{M}_a^*$ that corresponds to the same response of the sensors becomes

$$y_{mo,i} = \eta^*(t, x^*) = \Delta T \cdot T^*\left(x_i^*, y_i^*, z_i^*, t/\tau_{diff}, R, u(x,y,t)/\Delta T, H, \ell_x^*, \ell_y^*\right) + T_\infty \tag{1.68}$$

where the new list x^*, gathering the variables necessary for calculating the temperature response at a given time t, comprises one less parameters than the original x list (1.67):

$$x^* = \{\boldsymbol{\beta}^*, u, \Delta T, T_\infty\} \quad \text{with } \boldsymbol{\beta}^* = ((x_i^*, y_i^*, z_i^*) \quad \text{for } i = 1 \text{ to } q), \tau_{diff}, R, H, \ell_x^*, \ell_y^*) \tag{1.69}$$

1.6.2.2 2D Model in X- and Z-Directions

Model $\boldsymbol{M_a}$ can be simplified: if one knows that stimulus u does not vary much in direction y, or if the sensor whose response has to be simulated is not a point sensor but integrates the temperature signal in this direction, a y-direction average temperature field T_b can be rebuilt, with the definition of a new model $\boldsymbol{M_b}$ (see Figure 1.22b):

$$T_b(x,z,t) = \frac{1}{\ell_y}\int_0^{\ell_y} T_a(x,y,z,t)\,\mathrm{d}y \tag{1.70}$$

This 2D temperature field is produced by a source that varies in one single space direction, instead of two previously. This new source $u_m(x,t)$ does not depend on y and, as temperature, is the mean, in this direction, of the previous stimulus:

$$u_m(x,t) = \frac{1}{\ell_y}\int_0^{\ell_y} u(x,y,t)\,\mathrm{d}y \tag{1.71}$$

This mean temperature field verifies the following equations:

$$\frac{\partial^2 T}{\partial x^2} + \frac{\partial^2 T}{\partial z^2} = \frac{1}{a}\frac{\partial T}{\partial t} \tag{1.72}$$

$$T = T_0 \quad \text{at } t = 0, \quad \frac{\partial T}{\partial x} = 0 \quad \text{in } x = 0, \ell_x \tag{1.73}$$

$$-k\frac{\partial T}{\partial z} = u_m(x,t) \quad \text{at } z = 0; \quad -k\frac{\partial T}{\partial z} = h(T - T_\infty) \quad \text{at } z = e \tag{1.74}$$

Once put in a dimensionless form, this $\boldsymbol{M_b}$ model comprises $(2q + 7)$ independent variables:

$$x = \{\boldsymbol{\beta}, u_m, \Delta T, T_\infty\} \quad \text{with } \boldsymbol{\beta} = \left((x_i{}^*, z_i{}^* \quad \text{for } i = 1 \text{ to } q), \tau_{diff}, R, H, \ell_x^*\right) \tag{1.75}$$

Let us note now that in order for this model to show really no bias for sensor i, this detector should not be a point sensor, but a line sensor.

This is possible if the rear face ($z_i^* = 1$) temperature field is measured by infrared thermography. In that case, output of model $\boldsymbol{M_b}$ at location (x_i, y_i) is

$$y_{mod,i}(t_k) = T_b(x_i, z_i = e, t_k) \tag{1.76}$$

Its experimental counterpart can be scrutinized: one notes now $T_k^{\exp}(x^m, y^j)$ the temperature signal at time t_k, for pixel (x^m, y^j) of the infrared frame, where (m, j) designates a pixel located in the mth line and jth column.

The output (y-averaged) temperatures of the model have to be compared with the corresponding experimental response $y_i(t_k)$ of the ith detector: this can be obtained through simple addition:

$$y_i(t_k) = \frac{1}{n_i} \sum_{j=1}^{n_i} T_k^{\exp}(x^m, y^j = y_i) \tag{1.77}$$

where n_i is the number of pixels in the ith column (constant x^m). The reader should not be confused by the present notation in Equation 1.77: $y_i(t_k)$ is the experimental temperature signal of the ith detector, while y_i is its coordinate, in the y-direction.

If the average temperature in the y-direction is really measured by a line sensor, there will be no model error in the estimation of $u_m(x, t)$. However, the information on the variation of u in the y-direction is lost by this reduced modeling, which means that the description of u will be made with no resolution in this direction: people in charge of this estimation would have therefore to reduce also their initial objective, that is, estimation of $u_m(x, t)$ instead of $u(x, y, t)$.

1.6.2.3 1D Model in Z-Direction

Such an averaging can be pursued if one considers now the averaged value of the source over the whole front face area. The same type of averaging is made for the temperature field. This leads to model $\boldsymbol{M_c}$, shown in Figure 1.22c:

$$u_{mm}(t) = \frac{1}{\ell_x} \int_0^{\ell_x} u_m(x, t)\, \mathrm{d}x \tag{1.78}$$

$$T_c(z, t) = \frac{1}{\ell_x} \int_0^{\ell_x} T_b(x, z, t)\, \mathrm{d}x \tag{1.79}$$

$$\frac{\partial^2 T}{\partial z^2} = \frac{1}{a} \frac{\partial T}{\partial t} \tag{1.80}$$

$$T = T_0 \quad \text{for } t = 0 \tag{1.81}$$

$$-k \frac{\partial T}{\partial z} = u_{mm}(t) \quad \text{at } z = 0; \quad -k \frac{\partial T}{\partial z} = h(T - T_\infty) \quad \text{at } z = e \tag{1.82}$$

Once model $\boldsymbol{M_c}$ is put in a dimensionless form, only $(q+6)$ independent variables remain in the x list:

$$x = \{\boldsymbol{\beta}, u_{mm}, \Delta T, T_\infty\} \quad \text{with } \boldsymbol{\beta} = \left((z_i^*, \quad \text{for } i = 1 \text{ to } q), \tau_{diff}, R, H\right) \tag{1.83}$$

This reduction in the number of variables is made at the expense of the space resolution for u that is completely lost here since it is replaced by its space average u_{mm}.

1.6.2.4 2D Fin Model in X- and Y-Directions

If the Biot number $H = he/k$ is much lower than unity, temperature variations in the z-direction, corresponding to the slab thickness, can be considered as negligible and, consequently, heat transfer in the slab becomes two-dimensional (2D). The resulting 2D temperature field stems from an integration, with respect to z, of the 3D temperature field (see Figure 1.22d):

$$T_d(x, z, t) = \frac{1}{e} \int_0^e T_a(x, y, z, t)\, \mathrm{d}z \tag{1.84}$$

This reduced model $\boldsymbol{M_d}$ corresponds to a 2D fin whose temperature verifies the following equations:

$$\frac{\partial^2 T}{\partial x^2} + \frac{\partial^2 T}{\partial y^2} - \frac{h(T - T_\infty)}{ke} + \frac{u(x, y, t)}{ke} = \frac{1}{a} \frac{\partial T}{\partial t} \tag{1.85}$$

$$T = T_0 \quad \text{at } t = 0 \tag{1.86}$$

$$\frac{\partial T}{\partial x} = 0 \quad \text{in } x = 0, \ell_x; \quad \frac{\partial T}{\partial y} = 0 \quad \text{in } y = 0, \ell_y \tag{1.87}$$

List x is now composed of $(2q+8)$ independent variables:

$$x = \{\boldsymbol{\beta}, u, \Delta T, T_\infty\} \quad \text{with } \boldsymbol{\beta} = \left((x_i^*, y_i^* \text{ for } i = 1 \text{ to } q), \tau_{diff}, R, H, \ell_x^*, \ell_y^*\right) \tag{1.88}$$

This relatively high number of variables allows however to keep the initial spatial resolution of stimulus u.

1.6.2.5 1D Fin Model in X-Direction

The 2D-reduced model $\boldsymbol{M_b}$ can be used now to construct a 1D fin model, noted $\boldsymbol{M_e}$, with the same condition on the Biot number H, through an integration in the z-direction (the same model $\boldsymbol{M_e}$ can be obtained through integration of model $\boldsymbol{M_d}$ in y-direction [see Figure 1.22e]):

$$T_e(x, t) = \frac{1}{e} \int_0^e T_b(x, z, t)\, \mathrm{d}z \tag{1.89}$$

$$\frac{\partial^2 T}{\partial x^2} - \frac{h(T - T_\infty)}{ke} + \frac{u(x, y, t)}{ke} = \frac{1}{a}\frac{\partial T}{\partial t} \tag{1.90}$$

$$T = T_0 \quad \text{at } t = 0 \tag{1.91}$$

$$\frac{\partial T}{\partial x} = 0 \quad \text{in } x = 0, \ell_x \tag{1.92}$$

List x of the independent variables of the model is composed of $(q+7)$ quantities:

$$x = \{\boldsymbol{\beta}, u_m, \Delta T, T_\infty\} \quad \text{with } \boldsymbol{\beta} = \left(\left(z_i^* \quad \text{for } i = 1 \text{ to } q\right), \tau_{diff}, R, H, \ell_x^*\right) \tag{1.93}$$

1.6.2.6 0D Lumped Model

If the source is nearly uniform in space, with a low Biot number in direction z, or if the sensor provides the volume-averaged temperature of the slab, one obtains a 0D $\boldsymbol{M_f}$ model, also called lumped model or « small body » model. It corresponds to integration of model $\boldsymbol{M_e}$ in x-direction (see Figure 1.22f):

$$T_f(t) = \frac{1}{\ell_x}\int_0^e T_e(x, t)\,\mathrm{d}x \tag{1.94}$$

This temperature field is produced by a point source whose intensity $u_{mm}(t)$ varies with time, with

$$u_{mm}(t) = \frac{1}{\ell_x}\int_0^{\ell_x} u_m(x, t)\,\mathrm{d}x \tag{1.95}$$

The heat equation becomes

$$\rho ce\frac{\mathrm{d}T}{\mathrm{d}t} + h(T - T_\infty) = u_{mm}(t) \tag{1.96}$$

The x list of this model is now composed of only five independent variables, including a convective resistance (based on a unit area) $G = 1/h$ and a time constant $\tau = \rho ce/h = \tau_{diff}/H$:

$$x = \{\boldsymbol{\beta}, u_{mm}, \Delta T, T_\infty\} \quad \text{with } \boldsymbol{\beta} = (\tau, G) \quad \text{and} \quad \Delta T = T_0 - T_\infty \tag{1.97}$$

An analytical solution can easily be found:

$$T = T_\infty + \Delta T\,\exp\left(\frac{-t}{\tau}\right) + \frac{G}{\tau}\int_0^t u_{mm}(t')\,\exp\left(-\frac{t - t'}{\tau}\right)\mathrm{d}t' \tag{1.98}$$

This model is a limit model, only valid if the Biot number, based on the largest of the three dimensions ℓ_x, ℓ_y or e, is much lower than unity. If not, it is a biased model, but its output T_f can always be compared to the average temperature of the q sensors. This averaged experimental temperature brings an interesting information on the time variation of the average absorbed power density on the front face, $u_{mm}(t)$.

1.6.2.7 1D Local Model

A last model, noted $\boldsymbol{M_g}$ here, can be used. It is a 1D « local » temperature defined by

$$y_{mo,i} = T_g(x_i, y_i, t) = T_c(z_i, t; u(x_i, y_i, t), \Delta T, T_\infty, \boldsymbol{\beta}) \tag{1.99}$$

with

$$\boldsymbol{\beta}_i = (z_i^*, \tau_{diff\,i}, R_i, H_i) \tag{1.100}$$

It corresponds to the previous 1D model $\boldsymbol{M_c}$, applied locally for each sensor. Its response depends on the sole excitation $u(x_i, y_i, t)$ that prevails on the front face at the same (x, y) location (see Figure 1.23).

This allows considering a 3D problem as a set of independent 1D problems, each individual problem being associated to a specific sensor. Structural parameters belonging to vector $\boldsymbol{\beta}_i$ differ for each sensor. This vector is composed of a diffusion characteristic time $\tau_{diff\,i}$, a resistance R_i, and a Biot number H_i that have all local values corresponding to location of sensor i. These structural parameters are related to local thickness e_i, local heat transfer coefficient h_i, and local conductivity k_i and diffusivity a_i.

For the whole set of sensors, this model is composed of $(q + 6)$ independent variables if these sensors are embedded at the same depth in the slab and if the thermophysical parameters, h, and the slab thickness do not vary in the x–y plane.

This model is valid only if heat transfer is negligible in the directions of this same plane, that is, if the slab is made of a composite material that is homogenized but anisotropic: the principal directions of conductivity tensor $\overline{\overline{k}}$ should be those of the slab, with principal

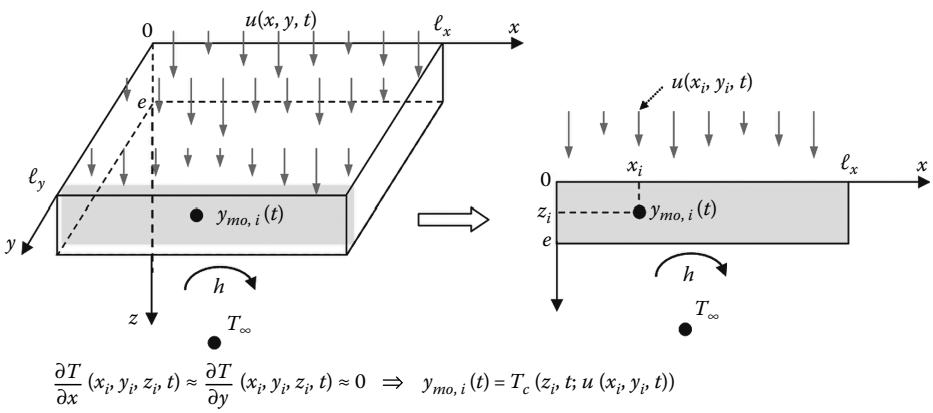

FIGURE 1.23
1D local model M_g.

components $k_x = k_y = 0$, $k_z = k$. However, it is possible to use it with a reasonable bias for sensors facing front face locations where stimulus u does not vary much (low gradient in the plane of this face) and for low thickness and thermophysical local variations. This model is also very interesting in nondestructive testing of composite slabs by infrared thermography (see Benítez et al. [2008]).

Remarks

- The six reduced models $\boldsymbol{M_b}$ to $\boldsymbol{M_g}$ are all derived from the detailed model $\boldsymbol{M_a}$ and have lower order dimensions than this original 3D model. They are also characterized by a lower number of structural parameters (see Chapters 13 and 14 for more details concerning the model reduction).
- Structural parameters of the slab and of the sensors either disappear or are transferred from one model to a more reduced one along this progressive physical reduction process. So, passing from model $\boldsymbol{M_e}$ to model $\boldsymbol{M_f}$ makes parameter ℓ_x^*, R, and x_i^* disappear while parameters H and τ_{diff} merge into a single parameter $\tau = \tau_{diff}/H$. This reduction of the parameters number is an irreversible one, which means that it is not possible to rebuild values of H and τ_{diff} starting from the knowledge of τ only.
- One can also note that during this reduction process, relationships between former and new parameters are linear if the logarithms of these parameters are considered: $\ln(\tau) = \ln(\tau_{diff}) - \ln(H)$. This gives an interesting relationship between reduced sensitivities (see the corresponding course in this series).
- In parallel with the reduction in the number of parameters, a reduction of the space dimension necessary for reproducing the sensor behavior appears: from an initial $u(x, y, t)$ stimulus for models $\boldsymbol{M_a}$ and $\boldsymbol{M_d}$, one gets a $u_m(x, t)$ stimulus for models $\boldsymbol{M_b}$ and $\boldsymbol{M_e}$ to finally $u_{mm}(t)$ for models $\boldsymbol{M_c}$ and $\boldsymbol{M_f}$ and $u_i(t) = u(x_i, y_i, t)$ for model $\boldsymbol{M_g}$.
- All these models rely on specific physical assumptions, and none of them corresponds to the absolute reality, even model $\boldsymbol{M_a}$: this one neglects convecto-radiative losses on the front face and on the four sides of the slab, coefficient h is supposed to be uniform in the rear face plane, and the same is true for the initial temperature inside the slab.

This example shows that the user has to make his or her own choice for the model, since several representations are generally possible. Accordingly, a more reduced model conveys less information about the spatial distribution of the heat source. However, this inconvenience in direct modeling can become an asset when inversion to reconstruct the source takes place.

1.6.3 Linear Input–Output Systems and Heat Sources

This section is devoted to the definition of what can be considered as a thermal power stimulus u. It can be later used for the purpose of estimating u, in an inversion procedure.

It has been shown above, for two geometries, semi-infinite medium (Example 1), and plane wall (Example 2), that the system-forced response u, to a surface heat flux stimulus, can be written, for any point P inside the medium, as a convolution product in time (see Equations 1.39 and 1.96), with a degenerate lumped body model in the second case.

In a very similar way, a continuous stimulus, that is, a power volumetric density, $u(\mathrm{P}, t)$, once discretized in space (or, more generally parameterized, using any basis of functions in 3D) as an input vector $\boldsymbol{U}(t)$, yields a forced response, in any point of the system, that corresponds to a convolution product in time, if the heat equation as well as its associated conditions are linear, with coefficients that can vary in space (nonhomogeneous system), but not in time (time invariant system). Let us notice that we consider only, in this section, linear heat sources, that is, sources that do not depend on state, here temperature, in the system.

This very general result can be applied to such a system in the specific case of a stimulus u whose time dependency can be separated from its space dependency:

$$u(\mathrm{P}, t) = f(t)g(\mathrm{P}) \tag{1.101}$$

We assume here that the source intensity (W m^{-3}) is associated to its time component $f(t)$, while its distribution in space $g(\mathrm{P})$ is its characteristic function (no unit): its value is 1, if point P belongs to the source and zero otherwise.

If the model is linear (in terms of the input/output relationship) and if its coefficients do not vary with time, model response $y_{mo,i}(t)$ at time t, in any point P_i in the system, can be written as a convolution product (Ozisik, 1980), for a zero initial temperature:

$$y_{mo,i}(t) = \int_0^t \int_V Z(t - \tau, \mathrm{P}_i; g(\mathrm{P}), \boldsymbol{\beta}) f(\tau)\, \mathrm{d}V(\mathrm{P})\, \mathrm{d}\tau \tag{1.102}$$

In this equation, Z is a transfer function (impedance or space Green's function) that depends on location of the observed point P_i, on the model structural quantities, as well as on the space distribution $g(\mathrm{P})$ of the source, P being any point inside the system. The convolution product is implemented between this impedance and the intensity $f(t)$ of the source.

If stimulus $u(\mathrm{P}, t)$ cannot be separated into a product of space and time distributions, this means that several different sources coexist in the system. Each of them can be ''separated'' and is noted $u_k(\mathrm{P}, t) = f_k(t)g_k(\mathrm{P})$, where k is the number of the individual source. One can think, for example, of two heating electrical resistances, embedded in a solid, and that are not turned on at the same time. So, a superposition of solutions of the previous form (1.102) can be implemented to get the global response in point P_i:

$$u(\mathrm{P}, t) = \sum_k f_k(t)g_k(\mathrm{P}) \tag{1.103}$$

$$y_{mo,i}(t) = \sum_k \int_0^t \int_V Z_k(t - \tau, \mathrm{P}_i; g_k(\mathrm{P}), \boldsymbol{\beta}) f_k(\tau)\, \mathrm{d}\tau\, \mathrm{d}V(\mathrm{P}) \tag{1.104}$$

Forms (1.102) and (1.104) remain valid in the quite general case where thermophysical properties of the constitutive materials, as well as the heat transfer coefficients and interface resistances used in the model, vary in space (system composed of heterogeneous materials).

However, if these parameters vary with time, the heat equation and its associated conditions may be still linear, but convolution products or transfer functions cannot be used for calculating the sensor responses anymore.

Nomenclature

a	thermal diffusivity ($m^2\ s^{-1}$)
$\vec{a}$	acceleration ($m\ s^{-2}$)
$\boldsymbol{A}$	state matrix
b	thermal effusivity ($J\ s^{1/2}\ m^{-2}\ K^{-1}$)
$\boldsymbol{B}$	input matrix
c, c_p	specific heat ($J\ kg^{-1}\ K^{-1}$)
$\boldsymbol{C}$	output matrix
D	diameter (m)
e	thickness (m)
E	energy (J)
$E(\dots)$	vector function
exp(.)	exponential of a matrix
f(.)	function (for time variable)
$\vec{F}$	force (N)
g(.)	function (for space variable)
G	coupling factor for the two-temperature model ($W\ m^{-3}\ K^{-1}$) or convective thermal resistance for a unit area of 0D lumped model ($m^2\ K\ W^{-1}$)
G(.)	Green's function
grad(.)	gradient vector
h	heat transfer coefficient ($W\ m^{-2}\ K^{-1}$)
$\hbar$	Planck's constant (J s)
H	Biot number, or enthalpy by unit volume ($J\ m^{-3}$)
k	thermal conductivity ($W\ m^{-1}\ K^{-1}$)
k_B	Boltzmann's constant ($J\ K^{-1}$)
$\vec{k}$	wave vector (m^{-1})
$\overline{\overline{k}}$	conductivity tensor, or thermal dispersion tensor ($W\ m^{-1}\ K^{-1}$)
K	thermal conductance for a unit area ($W\ m^{-2}\ K^{-1}$)
$\mathbf{K}$	macroscopic conductivity tensor of the two-temperature model ($W\ m^{-1}\ K^{-1}$)
ℓ, L	length (m)
m	number of data samples, or mass (kg)
$\boldsymbol{M}$	model
n	number of parameterized input function components
N	size of the state vector
N_q	distribution function for mode q
N_j	square of the function f_j norm
p	dim($\boldsymbol{B}$), or Laplace parameter (s^{-1})
$\mathrm{P} = (x, y, z)$	point coordinates
q	number of measurement points
q_{vol}	distributed volumic heat source ($W\ m^{-3}$)
$\vec{r}$	position vector
R	thermal resistance per unit area ($m^2\ K\ W^{-1}$)
t	time (s)
t_c	characteristic time (s)
t'	dumb integration variable (s)
T	temperature (K)
T_0	initial temperature (K)

T_∞	temperature of the fluid environment (K)
$T(t)$	column-vector of the discretized state (temperature)
$T_P(t)$	state (temperature) of the system, continuous version
$u(.)$	single input function (W m^{-2} or W m^{-3})
$\boldsymbol{u}_{param}$	single input parameterized vector
$\boldsymbol{U(t)}$	inputs column-vector (dim p)
$\vec{v}$, $\boldsymbol{v}$	velocity vector (m s^{-1})
x	list of data of direct problem
$\boldsymbol{x}$	data list for the direct problem
y	measured signal (output of a single sensor)
y_{mo}	theoretical signal, output of a model
$\boldsymbol{y}$	experimental output column-vector (dim m)
$\boldsymbol{y}_{mo}$	simulated column-vector (dim m)
Z	thermal impedance (m^2 K J^{-1})

Greek Variables

$\boldsymbol{\beta}$	parameter vector
χ	characteristic function
ΔT	temperature difference (K)
ε	volume fraction or porosity, or measurement noise
ε_i	noise at time t_i (K)
$\eta(.)$	function, output model structure
$\boldsymbol{\eta}(.)$	multiple-output model structure
λ	wavelength (m)
Λ	mean free path (m)
∇	nabla operator (gradient)
ϕ	heat flux (W)
$\vec{\varphi}$	heat flux density (W m^{-2})
ρ	mass density (kg m^{-3})
τ	time constant or relaxation time (s)
τ_{diff}	characteristic diffusion time (s)
Θ_D	Debye's temperature (K)

Subscripts

c	complementary (known)
calib	calibration
det	relative to a detailed model
e	electron
H	enthalpic
l	lattice
m	space average
mm	double space average
mo	model
n	normal
0	initial
param	parameterized
pos	position

P	relative to point P
q	mode number
r	researched
red	relative to a reduced model
s	sensor
ss	steady state
struct	structural
t	total
th	thermal
x	direction *x*
y	direction *y*
z	direction *z*
β	β-phase
λ	relative to wavelength λ
σ	σ-phase

Superscripts

$\bar{}$	time Laplace transform
$=$	tensor
*	exact value, or dimensionless quantity of a dimensionless model
T	transposed matrix

References

Anisimov, S.I., B.L. Kapeliovich, and T.L. Perel'man. 1974. *Zh. Eksp. Teor. Fiz*. **66**, 776.

Anisimov, S.I., B.L. Kapeliovich, and T.L. Perel'man. 1975. *Sov. Phys. JETP* **39**, 375.

Auriault, J.L. and H.I. Ene. 1994. Macroscopic modelling of heat transfer in composites with interfacial thermal barrier. *Int. J. Heat Mass Transf*. **37**(18), 2885–2892.

Battaglia, J.L., A. Kusiak, C. Rossignol, and N. Chigarev. 2007. Thermal diffusivity and effusivity of thin layers using the time-domain thermoreflectance. *Phys. Rev. B* **76**, 184110.

Benítez, H.D., C. Ibarra-Castanedo, A. Bendada, X. Maldague, H. Loaiza, and E. Caicedo. 2008. Definition of a new thermal contrast and pulse correction for defect quantification in pulsed thermography. *Infrared Phys. Technol*. **51**(3), 160–167.

Carbonell, R.G. and S. Whitaker. 1984. Heat and mass transfer in porous media. In: *Fundamentals of Transport Phenomenon Porous Media*, eds. J. Bear and M.Y. Corapcioglu, pp. 121–198. Dordrecht, the Netherlands: Martinus Nijhof.

Fourier, J. 1828. Mémoire sur la théorie analytique de la chaleur. http://www.academie-sciences.fr/membres/in_memoriam/Fourier/Fourier_pdf/Mem1828_p581_622.pdf

Frenkel, D. and S. Berend. 1996. *Understanding Molecular Simulation*. San Diego, CA: Academic Press.

Girault, M., D. Maillet, F. Bonthoux, B. Galland, P. Martin, R. Braconnier, and J.-R. Fontaine. 2008. Estimation of time-varying pollutant emission rates in a ventilated enclosure: Inversion of a reduced model obtained by experimental application of the modal identification method. *Inverse Probl*. **24**(February), 01 5021, 22.

Gobbé C., J.-L. Battaglia, and M. Quintard. 1998. Advanced concepts and techniques in thermal modelling, In: *Proceedings of Eurotherm Seminar No. 53*, Elsevier, (ed.), pp. 75–82, Mons, Belgium.

Maillet, D., S. André, J.C. Batsale, A. Degiovanni, and C. Moyne. 2000. *Thermal Quadrupoles—Solving the Heat Equation through Integral Transforms*. Chichester, U.K.: Wiley.

Maillet, D., A.S. Houlbert, S. Didierjean, A.S. Lamine, and A. Degiovanni. 1993. Nondestructive thermal evaluation of delaminations inside a laminate—Part I: Identification using the measurement of a thermal contrast and Part II: The experimental Laplace transforms method. *Compos. Sci. Technol*. **47**(2), 137–154, 155–172.

Moyne, C., S. Didierjean, H.P. Amaral Souto, and O.T. Da Silveira. 2000. Thermal dispersion in porous media: One equation model. *Int. J. Heat Mass Transf.*, **43**, 3853–3867.

Orlande, H.R.B., M.N. Ozisik, and D.Y. Tzou. 1995. Inverse analysis for estimating the electron-phonon coupling factor in thin metal films. *J. Appl. Phys*. **78**(3), 1843–1849.

Ozisik, M.N. 1980. *Heat Conduction*. Chichester, U.K.: Wiley.

Press, W.H., B.P. Flannery, S.A. Teulkosky, and W.T. Vetterling. 1992. *Numerical Recipes—The Art of Scientific Computing*. New York: Cambridge University Press.

Quintard, M., M. Kaviany, and S. Whitaker. 1997. Two-medium treatment of heat transfer in porous media: Numerical results for effective properties. *Adv. Water Resour*. **20**, 11–94.

Rémy, B. and A. Degiovanni. 2005. Parameters estimation and measurement of thermophysical properties of liquids. *Int. J. Heat Mass Transf*. **48**(19–20), 4103–4120.

Testu, A., S. Didierjean, D. Maillet, C. Moyne, T. Metzger, and T. Niass. 2007. Thermal dispersion coefficients for water or air flow through a bed of glass beads. *Int. J. Heat Mass Transf*. **50**(7–8), 1469–1484.

Volz, S. (Ed.). 2007. Microscale and nanoscale heat transfer. *Top. Appl. Phys*. **107**, 333–359.

2

Multiscale Modeling Approach to Predict Thermophysical Properties of Heterogeneous Media

Manuel Ernani Cruz and Carlos Frederico Matt

CONTENTS

2.1 Introduction

The purpose of this chapter is twofold: first we present, in a didactic form, the main ideas underlying the method of homogenization (also called homogenization theory) and, second, we use the method as a tool to develop a multiscale modeling approach, able to analyze a wide spectrum of transport phenomena in random heterogeneous media (media whose microstructures may be described appropriately by non-trivial joint probability density functions [JPDFs]). The approach is also based on variational calculus and the finite element method and leads to the prediction of macroscopic effective properties of heterogeneous media. Here, the multiscale approach is exposed in the context of the heat conduction problem in composite materials, whose components are all thermally conducting. An expression for the tensorial effective thermal conductivity of such materials is derived, and some properties of the effective conductivity are shown.

In this chapter, we present in detail the continuous formulations of the heat conduction problems, which are part of the multiscale approach. On the other hand, we only summarize the main steps for numerical solution of these problems via the finite element method. Sample numerical results for the effective thermal conductivity of the 2D square array of circular cylindrical fibers and of the 3D simple cubic array of spheres are presented up to maximum packing. The reader is referred to the works by Cruz and Patera (1995), Cruz et al. (1995), Cruz (1997, 1998), Machado and Cruz (1999), Matt (1999, 2003), Rocha (1999), Machado (2000), Rocha and Cruz (2001), Matt and Cruz (2001, 2002a, 2002b, 2004, 2006, 2008), and Pereira et al. (2006) for more details of the numerical solutions and for the presentations and analyses of numerical results for the effective thermal conductivities of 2D and 3D, ordered and random composites. Various computational techniques developed to address the heat conduction problem in composite materials are reviewed by Pereira et al. (2006), Matt and Cruz (2006, 2008), and Cruz (2001).

It should be remarked that there are several other approaches to analyze transport phenomena in heterogeneous and multiphase systems. Phenomenological effective medium approaches (see Torquato 2002) do not tackle the underlying physics at the microstructural level, such that they attempt to establish the macroscopic properties by proposing ad hoc assumptions. Another much employed technique is volume averaging, as discussed in Chapter 1 and in the monograph by Whitaker (1999). The main objective of volume averaging is to formulate the spatially smoothed governing equations that are valid everywhere in the heterogeneous medium of interest. The development of closure problems is then necessary to permit the prediction of the medium's effective transport properties, which relate macroscopic fluxes to intensity gradients. Regarding both volume averaging and homogenization approaches, it appears that much more research effort has been devoted to formulating several different classes of transport problems in heterogeneous media than to computing the associated macroscopic properties. Therefore, a comparative analysis of effective property results arising from these alternative methods is beyond the scope of the present work.

The outline of this chapter is as follows. In Section 2.2, the method of homogenization is introduced didactically. We first offer a formal definition and then illustrate with physical examples the mathematical problems involved in the definition. Next, we give a brief overview of the analytical techniques that may be employed in the homogenization procedure. Finally, we apply the method to a general elliptic model problem in strong form.

In Section 2.3, we apply the method of homogenization to the heat conduction problem of interest, adopting a variational approach and exploiting the analysis of Section 2.2. Although some of our results are also shown, in a different form, in Auriault (1983), we not only present a more detailed derivation here, but also the variational treatment makes the final expressions directly suitable for subsequent numerical treatment using the finite element method. In Sections 2.4 through 2.7, we describe the multiscale modeling approach, which decomposes the original multiscale problem into the macroscale, mesoscale, and microscale (sub)problems. In Section 2.8, we briefly discuss the numerical treatment of the pertinent problems, and in Section 2.9 we present some representative results stemming from solutions to the mesoscale and microscale problems. Finally, in Section 2.10, we state the conclusions.

2.2 Method of Homogenization

The method of homogenization can be applied to analyze a variety of periodic heterogeneous systems—those composed of several macroscopic phases and/or dissimilar constituents and characterized by a repetitive elementary structure. A comprehensive treatment of the subject is given in Bensoussan et al. (1978), and a survey of applications of homogenization theory to a wide spectrum of problems can be found in Babuška (1975). The method has been applied to study neutron and radiative transport (Larsen 1975, Bensoussan et al. 1979), to tackle the problem of dynamic fluid–structure interactions in large rod bundles (Schumann 1981) and to develop a procedure for shape optimization of structures (Bendsøe and Kikuchi 1988). In Mei and Auriault (1989), the method is the essence of the formulation of the creeping flow problem through periodic porous media with several spatial scales, and in Mei and Auriault (1991) the approach is extended to include the effect of weak inertia. Kamiński and Kleiber (2000) have also employed homogenization to investigate the behavior of random elastic composites with stochastic interface defects.

In the heat transfer (or rather conduction) context, the objective is to determine the effective thermal conductivity of an equivalent homogeneous medium, which will thermally behave, in a macroscopic sense, as the original heterogeneous medium (Milton 2002). Auriault (1983) and Auriault and Ene (1994) have used homogenization to determine the effective conductivity of certain types of laminated composites. More recently, homogenization theory has been applied in Cruz (1998) to derive an expression for the effective conductivity of particulate composites whose continuous (the matrix) and dispersed (the particles) components are thermally conducting. The dependence of the thermal conductivity of composite materials on temperature has been considered in Chung et al. (2001) by applying homogenization.

2.2.1 Definition

In short, the method of homogenization employs volume averaging (see Chapter 1) to yield a mathematically rigorous mixture-type model for a heterogeneous medium with periodic microstructure and separated length scales. A formal definition may be offered by first introducing three types of boundary value problems (BVPs).

1. BVP-1

$$A^{\varepsilon}u_{\varepsilon} = f \quad \text{in } \Omega, \tag{2.1}$$

$$u_{\varepsilon} \text{ subject to boundary conditions on } \partial\Omega. \tag{2.2}$$

The domain Ω is an open bounded set of $\mathcal{R}^n$, $\partial\Omega$ is the bounding surface of Ω in $\mathcal{R}^{n-1}$, A^{ε} is a general partial differential operator with periodically varying and *continuous* coefficients, f: $\Omega \rightarrow \mathcal{R}^m$, $m \leq n$, is the source term, and u_{ε} is subject to Dirichlet, Neumann, and/or mixed boundary conditions in (2.2).

The characteristic length scales of the domain Ω and of the periods of the coefficients are, respectively, L and λ; the positive parameter ε is the ratio of such scales, and it is assumed here that the scales are well separated, that is,

$$\varepsilon \equiv \frac{\lambda}{L} \ll 1, \tag{2.3}$$

implying statistical homogeneity. BVP-1 is said to have rapidly oscillating coefficients.

2. BVP-2

$$A^{\mathrm{H}}u_{\mathrm{H}} = f \quad \text{in } \Omega, \tag{2.4}$$

$$u_{\mathrm{H}} \text{ subject to boundary conditions on } \partial\Omega. \tag{2.5}$$

The partial differential operator A^{H} has *constant* coefficients, that is, A^{H} is a homogeneous operator; thus, this BVP is said to be homogenized.

3. BVP-3

$$A^{\mathrm{C}}u_{\mathrm{C}} = f^{\mathrm{C}} \quad \text{in } \Omega^{\mathrm{C}}, \tag{2.6}$$

$$u_{\mathrm{C}} \text{ subject to boundary conditions on } \partial\Omega^{\mathrm{C}}. \tag{2.7}$$

The domain Ω^{C}, an open bounded set of $\mathcal{R}^n$, is a periodic cell of characteristic size λ, that is, with dimensions proportional to λ in all n coordinate directions. The partial differential operator A^{C} may have constant or variable coefficients within Ω^{C}, and u_{C} and f^{C} are λ-periodic functions (functions that admit period $C_j\lambda$, $C_j = O(1) \in \mathcal{R}$, in the direction x_j, $j = 1, \ldots, n$). This BVP is called a cell problem.

We are now in a position to offer a formal definition of the method of homogenization: the method is a rigorous mathematical technique whereby one can replace, in the limit $\varepsilon \rightarrow 0$, a BVP with rapidly varying coefficients (type BVP-1) with a homogenized problem (type BVP-2), whose coefficients must be determined through the solution of a cell problem (type BVP-3). Although all three problems are, in general, hard to solve analytically, the method of homogenization has the distinct advantage that problems of the types BVP-2 and BVP-3 are much easier to solve numerically than those of the type BVP-1, since the latter not only require $O(1/\varepsilon^n)$ more degrees of freedom but are also much stiffer.

From the point of view of physics, problem BVP-1 may describe heat transfer, creeping flow, or a neutron transport process in a heterogeneous medium of typical macroscale L with a spatially periodic microstructure of period λ. Problems BVP-2 and BVP-3 may describe the same aforementioned phenomena, respectively, in a homogeneous, effective

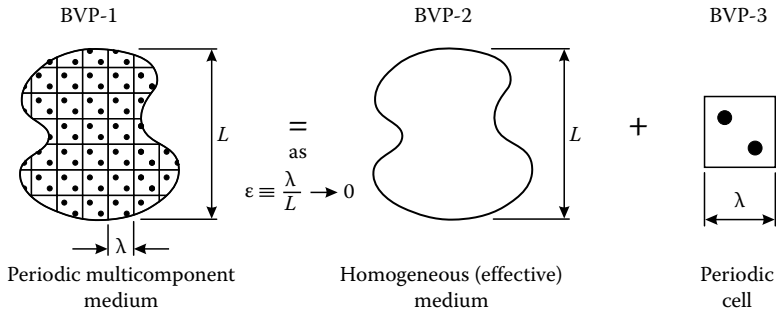

FIGURE 2.1
Diagrammatic representation of the method of homogenization.

medium (in general anisotropic) of typical macroscale L and in a periodic cell of size λ. Note that the coefficients of A^{H} in BVP-2 correspond, by definition, to the effective macroscopic properties of the original heterogeneous medium considered in BVP-1. Because the determination of such coefficients demands that a solution be found to a cell problem defined in the periodic microstructure of the medium, of size $\lambda \ll L$, it is said that the method of homogenization allows one to describe macroscopically the behavior of a heterogeneous medium through the analysis of the behavior of its underlying microscopic structure; Figure 2.1 illustrates this process.

The lack of a unique precise definition of effective property of a heterogeneous medium led to many reports in the past with discrepant results (Babuška 1975). The method of homogenization not only provides a consistent way of computing effective properties for heterogeneous materials with periodic microstructures, but it also relates global quantities (e.g., bulk heat flow) defined for the original medium to those computed for the equivalent homogeneous medium. It should be pointed out that, typically, real random heterogeneous media possess no period λ, in which case homogenization theory does not *directly* apply. The concept of the correlation length (Cruz and Patera 1995, Cruz 2005), developed in Section 2.6.4, may be used to bridge the transition *periodic* → *random*, provided such length is small compared to the macroscale L.

2.2.2 Additional Considerations

As previously discussed in Chapter 1, the elaboration of a mathematical model to describe a given physical phenomenon is relative to the desired scale of observation, and is a typical product of scientific investigation. Frequently, the model leads to a problem of the type BVP-1, particularly when one is dealing with heterogeneous systems; homogenization theory can thus be employed to solve such model. In order to replace the operator A^{ε} of BVP-1 with the operator A^{H} of BVP-2, several mathematical techniques can be used, based on (see, e.g., Bensoussan et al. 1978) the following:

1. Asymptotic expansions using multiple scales, the fast scale proportional to λ, and the slow scale proportional to L
2. Energy estimates
3. Probabilistic arguments
4. Spectral decomposition of A^{ε}

The method of asymptotic expansions is attractive when dealing with problems of the type BVP-1 because of the presence of a natural *separation of scales*, as evidenced by Equation 2.3; note that such clear separation of scales is not present in turbulence. The procedure is then to look for the solution $u_\varepsilon = u_\varepsilon(\mathbf{x})$, $\mathbf{x} \in \mathcal{R}^n$, of BVP-1 in the form of an asymptotic expansion in terms of the small positive parameter ε:

$$u_\varepsilon = u_0 + \varepsilon u_1 + \varepsilon^2 u_2 + \cdots, \tag{2.8}$$

where the functions u_j, $j = 0,1,\ldots$, are now the new unknowns, having all the same order of magnitude. Next, by inserting (2.8) into (2.1) and (2.2) and collecting equal powers of ε, a problem of the type BVP-2 is obtained for u_0, with boundary conditions dependent on those prescribed for the original problem. The main result of the method, shown by Bensoussan et al. (1978), is that u_ε converges weakly to u_0 as $\varepsilon \to 0$ (weak convergence means convergence of suitable averages). The explicit analytical construction of the homogeneous operator A^{H} is crucial for the actual solution of the problem and involves solving a λ-periodic cell problem (type BVP-3), which yields the correct constant coefficients of A^{H}. In general, the homogenized and cell problems have to be solved numerically. In the following section, we apply the asymptotic expansion technique to a typical elliptic model problem.

2.2.3 Application to a Model Problem

Let us apply the method of homogenization to the following model problem in strong form: in BVP-1, let

$$A^\varepsilon = -\frac{\partial}{\partial x_i}\left(a_{ij}(\mathbf{y})\frac{\partial}{\partial x_j}\right) + a_0(\mathbf{y}), \tag{2.9}$$

where $\mathbf{x} \in \mathcal{R}^3$, $\mathbf{y} \equiv \mathbf{x}/\varepsilon$, and $a_{ij}(\mathbf{y})$, $i, j = 1,2,3$, and $a_0(\mathbf{y})$ are continuous λ-triply periodic functions; we remark that the summation convention is adopted throughout this chapter. Formally, a function is said to be λ-triply periodic if it admits periods proportional to λ in all three coordinate directions. The second-order elliptic operator A^ε in (2.9) models many physical phenomena (e.g., heat or electrical conduction) in composite materials with periodic microstructure. We are now interested in determining the behavior of the solution u_ε of BVP-1, with A^ε given in (2.9), as $\varepsilon \to 0$.

The presence of the two disparate scales L and λ in BVP-1, and the λ-periodicity of A^ε motivate the application of the method of asymptotic expansions using multiple scales (Bensoussan et al. 1978, Mei and Auriault 1989), whereby we look for the solution $u_\varepsilon(\mathbf{x})$ in the form

$$u_\varepsilon(\mathbf{x}) = u_0\left(\mathbf{x}, \frac{\mathbf{x}}{\varepsilon}\right) + \varepsilon u_1\left(\mathbf{x}, \frac{\mathbf{x}}{\varepsilon}\right) + \varepsilon^2 u_2\left(\mathbf{x}, \frac{\mathbf{x}}{\varepsilon}\right) + \cdots, \tag{2.10}$$

where $u_j(\mathbf{x}, \mathbf{y})$, $\mathbf{y} \equiv \mathbf{x}/\varepsilon$, $j = 0, 1, 2, \ldots$, are λ-triply periodic in $\mathbf{y}$. The ''fast'' variable $\mathbf{y}$ scales (magnifies) the period λ to L and is introduced here to separate the periodic and nonperiodic parts of u_ε, which vary, respectively, rapidly over λ and slowly over L. The new BVPs for the unknown functions u_j are determined by first inserting (2.10) into (2.1), with A^ε given in (2.9), and then by collecting the terms with equal powers of ε. Note that care is necessary with the operator $\partial/\partial x_j$: when operating on a function $G = \hat{G}(\mathbf{x}) = \breve{G}(\mathbf{x}, \mathbf{y})$, we

must first treat **x** and **y** as independent variables, and subsequently replace **y** with $\mathbf{x}/\varepsilon$ to obtain

$$\frac{\partial}{\partial x_j}(G) = \frac{\partial \hat{G}}{\partial x_j} = \frac{\partial \breve{G}}{\partial x_j} + \frac{1}{\varepsilon}\frac{\partial \breve{G}}{\partial y_j}. \tag{2.11}$$

If, furthermore, G can be expanded as $G = G_0 + \varepsilon G_1 + \varepsilon^2 G_2 + O(\varepsilon^3)$, then from (2.11)

$$\frac{\partial}{\partial x_j}(G) = \frac{\partial \breve{G}_0}{\partial x_j} + \frac{1}{\varepsilon}\frac{\partial \breve{G}_0}{\partial y_j} + \varepsilon\frac{\partial \breve{G}_1}{\partial x_j} + \frac{\partial \breve{G}_1}{\partial y_j} + \varepsilon^2\frac{\partial \breve{G}_2}{\partial x_j} + \varepsilon\frac{\partial \breve{G}_2}{\partial y_j} + O(\varepsilon^2). \tag{2.12}$$

Inserting Equation 2.9 into 2.1, and using Equation 2.12, one obtains

$$A^{\varepsilon}u_{\varepsilon} = (\varepsilon^{-2}A_2 + \varepsilon^{-1}A_1 + \varepsilon^0 A_0)u_{\varepsilon} = f, \tag{2.13}$$

where

$$A_2 = -\frac{\partial}{\partial y_i}\left(a_{ij}(\mathbf{y})\frac{\partial}{\partial y_j}\right), \tag{2.14}$$

$$A_1 = -\frac{\partial}{\partial y_i}\left(a_{ij}(\mathbf{y})\frac{\partial}{\partial x_j}\right) - \frac{\partial}{\partial x_i}\left(a_{ij}(\mathbf{y})\frac{\partial}{\partial y_j}\right), \tag{2.15}$$

$$A_0 = -\frac{\partial}{\partial x_i}\left(a_{ij}(\mathbf{y})\frac{\partial}{\partial x_j}\right) + a_0. \tag{2.16}$$

Now inserting Equation 2.10 into 2.13, and collecting the powers ε^{-2}, ε^{-1}, and ε^0, the following equations involving A_0, A_1, A_2 and u_0, u_1, u_2 result:

$$A_2u_0 = 0, \tag{2.17}$$

$$A_2u_1 + A_1u_0 = 0, \tag{2.18}$$

$$A_2u_2 + A_1u_1 + A_0u_0 = f. \tag{2.19}$$

Before proceeding further, we state a result to be used in the development to follow. The *solvability condition* (i.e., uniqueness up to an additive constant) for the problem

$$\begin{cases} A_2\phi = F \text{ in } Y, \\ \phi \text{ periodic in } Y, \end{cases} \tag{2.20}$$

where A_2 is given in (2.14) and Y is a region in $\mathcal{R}^3$, is (see Bensoussan et al. 1978)

$$\int_Y F(\mathbf{y})\, d\mathbf{y} = 0. \tag{2.21}$$

To arrive at (2.21), we integrate (2.20) over Y, apply the first form of Green's theorem (Hildebrand 1976), and then use the periodicity of ϕ.

Noting that the operator A_2 involves $\mathbf{y}$ only, and considering the solvability condition (2.21), we conclude that Equation 2.17 implies that u_0 is a function of $\mathbf{x}$ only, that is,

$$u_0 = u_0(\mathbf{x}). \tag{2.22}$$

Inserting Equations 2.15 and 2.22 into 2.18, we obtain

$$A_2 u_1 = \left(\frac{\partial}{\partial y_i} a_{ij}(\mathbf{y})\right) \frac{\partial u_0(\mathbf{x})}{\partial x_j}; \tag{2.23}$$

the separation of the variables $\mathbf{x}$ and $\mathbf{y}$ on the right-hand side (RHS) of (2.23) allows one to represent u_1 in the following simple form: if $\chi^j = \chi^j(\mathbf{y})$ is defined as the λ-triply periodic solution (up to an additive constant) of

$$A_2 \chi^j = -\frac{\partial}{\partial y_i} a_{ij}(\mathbf{y}), \tag{2.24}$$

then the general solution of (2.23) is given by

$$u_1(\mathbf{x}, \mathbf{y}) = -\chi^j(\mathbf{y}) \frac{\partial u_0}{\partial x_j} + \tilde{u}_1(\mathbf{x}). \tag{2.25}$$

The problem for u_1 then reduces to finding $\chi^j(\mathbf{y})$; since A_2 involves $\mathbf{y}$ only and both $a_{ij}(\mathbf{y})$ and $\chi^j(\mathbf{y})$ are λ-triply periodic, Equation 2.24 (with proper boundary conditions) constitutes the *cell problem* BVP-3.

From the condition (2.21), it is easily seen that one can solve (2.19) for u_2, treating $\mathbf{x}$ as a parameter, if

$$\int_Y (A_1 u_1 + A_0 u_0)\, d\mathbf{y} = \int_Y f\, d\mathbf{y} \tag{2.26}$$

(note that, here, Y has dimensions proportional to λ in all coordinate directions); using (2.15), (2.16), and (2.25) and the fact that $f = f(\mathbf{x})$, (2.26) becomes

$$\int_Y \left\{ -\frac{\partial}{\partial y_i}\left(a_{ij}(\mathbf{y}) \frac{\partial u_1(\mathbf{x}, \mathbf{y})}{\partial x_j}\right) - \frac{\partial}{\partial x_i}\left(a_{ik}(\mathbf{y}) \frac{\partial}{\partial y_k}\left(-\chi^j(\mathbf{y}) \frac{\partial u_0}{\partial x_j} + \tilde{u}_1(\mathbf{x})\right)\right) - \frac{\partial}{\partial x_i}\left(a_{ij}(\mathbf{y}) \frac{\partial u_0}{\partial x_j}\right) + a_0 u_0 \right\} d\mathbf{y} = f \int_Y d\mathbf{y}, \tag{2.27}$$

or, since $\mathbf{x}$ is a parameter,

$$-\frac{1}{|Y|}\left\{\int_Y \left(a_{ij} - a_{ik}\frac{\partial \chi^j}{\partial y_k}\right) d\mathbf{y}\right\} \frac{\partial^2 u_0}{\partial x_i \partial x_j} + \frac{1}{|Y|}\left\{\int_Y a_0(\mathbf{y}) d\mathbf{y}\right\} u_0 = f, \tag{2.28}$$

where $|Y|$ is the measure of the entire region Y,

$$|Y| \equiv \int_Y d\mathbf{y}. \tag{2.29}$$

Clearly, the coefficients

$$C_{\text{eff}_{ij}} \equiv -\frac{1}{|Y|}\int_Y \left(a_{ij} - a_{ik}\frac{\partial \chi^j}{\partial y_k}\right) d\mathbf{y}, \tag{2.30}$$

and

$$C_0 \equiv \frac{1}{|Y|}\int_Y a_0(\mathbf{y}) d\mathbf{y} \tag{2.31}$$

are constants ($\mathbf{y}$ is integrated out); therefore, Equation 2.28 (with proper boundary conditions) constitutes the *homogenized problem* BVP-2. We can thus write the homogenized operator A^{H} explicitly as

$$A^{\text{H}} = C_{\text{eff}_{ij}}\frac{\partial^2}{\partial x_i \partial x_j} + C_0; \tag{2.32}$$

defining, in general, the average

$$m(\phi) \equiv \frac{1}{|Y|}\int_Y \phi(\mathbf{y}) d\mathbf{y}, \tag{2.33}$$

then

$$C_{\text{eff}_{ij}} = -m(a_{ij}) + m\left(a_{ik}\frac{\partial \chi^j}{\partial y_k}\right) \tag{2.34}$$

and

$$C_0 = m(a_0). \tag{2.35}$$

Mathematically, $C_{\text{eff}_{ij}}$ and C_0 are the *effective coefficients* of the operator A^{ε}; physically, they are the *effective bulk properties* of the heterogeneous medium, associated with the physical process for which BVP-1 is the appropriate model.

It is worthwhile to conclude this section by stating the following results, which are proved by Babuška (1975) and Bensoussan et al. (1978).

1. *Symmetry*. If A^{ε} is symmetric ($a_{ij} = a_{ji}$), then A^{H} is also symmetric.
2. *Ellipticity*. For our model problem, the operator A^{H}, which does not depend on Ω, is elliptic.